Theor Chem Account (2008) 119:155–176
DOI 10.1007/s00214-007-0276-8

REGULAR ARTICLE

A combined theoretical and experimental study of the structure and vibrational absorption, vibrational circular dichroism, Raman and Raman optical activity spectra of the L-histidine zwitterion

E. Deplazes · W. van Bronswijk · F. Zhu · L. D. Barron · S. Ma · L. A. Nafie · K. J. Jalkanen

Received: 22 December 2006 / Accepted: 20 February 2007 / Published online: 18 April 2007

Abstract A combined theoretical and experimental study of the vibrational absorption (VA)/IR, vibrational circular dichroism (VCD), Raman and Raman optical activity (ROA) spectra of L-histidine in aqueous solution has been undertaken to answer the questions (i) what are the species present and (ii) which conformers of the species are present under various experimental conditions. The VA spectra of L-histidine have been measured in aqueous solution and the spectral bands which can be used to identify both species (cation, zwitterion, anion) and conformer of the species have been identified and subsequently used to identify the species (zwitterion) and conformer (gauche minus minus, gauche minus plus for the side chain dihedral angles) present in solution at pH 7.6. The VCD spectral intensities have been used subsequently in combination with further theoretical studies to confirm the conclusions that have been arrived at by only analyzing the VA/IR spectra. Finally a comparison of measured Raman and ROA spectra of L-histidine with Raman and ROA spectral simulations for the conformers and species derived from the combined VA/IR and VCD experimental and theoretical work is presented as a validation of the conclusions arrived at from VA/IR and VCD spectroscopy. The combination of VA/IR and VCD with Raman and ROA is clearly superior and both sets of experiments should be performed.

Keywords L-histidine · IR · Conformational analysis · Hydration · Zwitterion · VCD · Raman and ROA

E. Deplazes · W. van Bronswijk · K. J. Jalkanen (✉)
Nanochemistry Research Institute,
Department of Applied Chemistry,
Curtin University of Technology,
P.O. Box U1987, Perth, WA 6845, Australia
e-mail: jalkanen@ivec.org

F. Zhu · L. D. Barron
Department of Chemistry, University of Glasgow,
Glasgow G12 8QQ, Scotland

S. Ma · L. A. Nafie
Department of Chemistry, Syracuse University,
Syracuse, NY 13244-4100, USA

1 Introduction

L-histidine (LH) is a polyprotic amino acid that plays an important part in many biological systems. In solution histidine exhibits five different protonation states depending on the pH of the system [1]. The ionic state ranges from the doubly protonated species in highly acidic solutions to the zwitterions at neutral pH to the doubly deprotonated state in alkaline solutions. Due to the two nitrogen atoms in the imidazole ring the zwitterion shows two tautomeric forms that exist in equilibrium at biological pH [2]. In addition to these protonation states histidine presents six different geometrical conformations that are defined by two dihedral angles χ_1 and χ_2 shown in Fig. 1.

As a direct consequence of this multi-faceted structure histidine exhibits a variety of functionalities in biological systems. It serves as a facilitator for proton transfer, forms the active residue in proteins and plays an active role in the mechanism of many enzyme reactions [3–6]. It acts as a donor and acceptor for hydrogen bonding [4,7] and so influences the secondary and tertiary structure of peptides, proteins and other large biomolecules. The imidazole ring is an important ligand for many metals such as Fe, Ni, Cu and Zn and histidine is often the active binding site in metalloproteins [8–11], which in turn are found in many biological systems such as haemoglobin, ferritin or the antioxidant super oxide dismutase. The binding of biological molecules is also of interest for research into biosensors and biocatalysis [8].

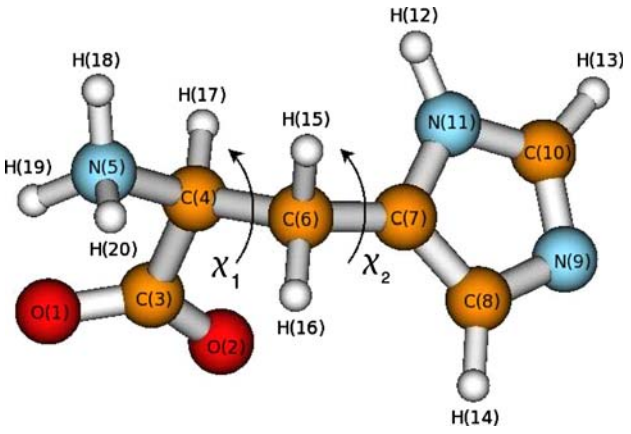

Fig. 1 Numbering scheme and definition of dihedral angles of the L-histidine zwitterion

Hence methods for the determination, systematic characterisation and prediction of the protonation states, tautomeric forms and conformers of histidine are useful in many areas such as the investigative studies of enzyme reactions, metalloproteins and the understanding and prediction of protein folding.

Infrared and Raman spectroscopy are suitable techniques to carry out structural investigation of amino acids and peptides. A change in the protonation state or geometrical conformation considerably affects the geometrical parameters such as bond lengths and angles as well as relative energies of the molecule and results in altered vibrational properties [1,2,8–10,12–17]. IR and Raman can be used to characterize the five protonation states [1,2,14,15] and tautomers [14] as well as the binding modes [9,10] of histidine. Due to the structural complexity of histidine the vibrational properties and binding modes are often studied using a model compound such as 4-methyl or 5-methylimidazole [16–18]. Other techniques used to study the structure of amino acids include NMR [19] and UV Resonance Raman spectroscopy (UVRR) [4–6,20]. Zhao et al. [21] showed that the proton level of an aggregation of histidine residues rather than of a single histidine molecule can be determined using UVRR.

The results of structural determination of amino acids and peptides by vibrational spectroscopy can be enhanced when combined with computational methods [2,22,23]. Theoretical studies give additional information on the geometries, relative energies and vibrational properties [24–29]. The results of calculated spectra can assist in band assignment and identifying characteristic properties for different structures and conformers [2,16,18,19,25]. When carrying out theoretical studies of amino acids and peptides in solution, the molecule should not be modelled in the gas phase, independent of the level of theory used for the calculations. An appropriate solvent model should be applied to account for the effect of solvation. A number of studies have shown that the effect of the solvent significantly changes the structure, relative energies and vibrational properties of a system [12,19,22,23,25,30–35]. Some structures are not even stable in the gas phase. Spectra that are calculated using an appropriate solvent model are often in better agreement with the experimental spectra than models in the gas phase. As the quantitative effect depends on the solvation model chosen [22,23,36], a number of different solvation models should be considered. A dielectric continuum model is suitable for the simulation of the bulk effect while explicit solvent molecules are used to model a hydrogen-bonded cluster surrounding the solute molecule. The position and number of water molecules in the first hydration shell can be determined by molecular dynamic simulations as reported in previous studies [25,31]. These calculations showed that the structural and spectral properties depend on the number and position of the solvent molecules. The structure of clustered water molecules and their packing efficiency in the hydration shell of peptides and proteins has also been the subject of a number of experimental studies [37,38]. X-ray and neutron scattering measurements showed that water in a hydration shell is denser than bulk water [37]. The configurations of water molecules at the protein-solvent interface show different configurations and volumes than the ones in the core of the system. NMR provides a complementary technique for the study of hydration in biological macromolecules [38]. Additionally the configurations adopted by water molecules have been analyzed by IR spectroscopic methods [39].

For organic molecules, where the explicit solvent molecules are not expected to change the topology of the potential energy surface (PES), the use of the continuum solvent models is probably adequate. But for biological systems solvent and ligand binding has been shown to change the conformation (secondary structure) [sometimes even the tertiary structure, the so-called allosteric effect] through H-bonding and charge transfer effects not included in the continuum solvent models. In addition, during ligand binding, the ligand displaces the H-bonded solvent molecules. So there is a competition between intramolecular H-bonding within the molecules and intermolecular H-bonding with the solvent molecules and the ligand. To model these very complex systems, the use of solvent molecules strongly interacting with the charged and polar groups may be required. In many cases this may require a 2–3 Å layer of explicit solvent molecules, as not all of the solvent molecules are directly H-bonded with the solute but are responsible for the positioning of the solvent molecules which do.

This study investigates the different structures of the LH zwitterion employing density functional theory (DFT) for geometrical optimisation and vibrational absorption (VA) spectra calculations. Further calculations focus on the dependence of the calculated spectra on the solvation model and level of theory used as well as the effect of deuterium substitution.

Reported pK_a values of LH have been used to identify five specific pHs at which one protonation state is in the highest fractional abundance possible. IR spectra have been collected at these pHs to identify and confirm the reported characteristic bands for each protonation state. Additionally the IR spectra of LH in a D_2O solution at pD 7.6 has been collected. These experimental spectra are used for comparison to and evaluation of the calculated spectra.

The effect of solvation on the structure and vibrational properties is investigated by applying five different solvation models to the zwitterion of LH. To the best of our knowledge LH has not been modeled in a solvated state but has mainly been studied using model compounds such as 4- and 5-ethylimidazole in the gas phase. This study attempts to apply the knowledge gained from previous studies of the solvation of amino acids such as L-alanine [26–28], L-alanyl-L-alanine [29,31], the alanine dipeptide [25,34,35] and tri-L-serine [23] to the LH zwitterion. To consider the bulk effect of the solvent a continuum dielectric model called "Conductor like Screening model" (COSMO), implemented in the Amsterdam Density Functional (ADF) package [40], and the "Polarizable Continuum Model" (PCM) in Gaussian were used. The stabilizing effect of hydrogen bonds formed by a cluster of individual water molecules is simulated by placing explicit solvent molecules around the histidine molecule, as we have done in previous works [25,31,34]. To combine the two effects the COSMO model is simply applied to the optimized structure containing the explicit water molecules. Models with different numbers of water molecules were used to test the dependence of the structure and its properties on the number of explicit solvent molecules added. The histidine molecule was solvated using the following five models: (i) LH + COSMO or PCM (LHC), (ii) LH + 13 water molecules (LH13), (iii) LH + 13 water molecules + COSMO or PCM (LH13C), (iv) LH + 17 water molecules (LH17) and (v) LH + 17 water molecules + COSMO or PCM (LH17C).

Initial structures for the six conformers of the LH zwitterion were optimized in the LHC, LH13 and LH13C models at the OPBE0/DZP level. The minimized structures were compared to investigate the effect of the solvation on the geometrical parameters and relative energies of the six conformers. The VA spectra were calculated for all of these structures and compared to identify the effect of solvation and test if the six conformers can be distinguished by their spectral properties. The experimental spectrum of the zwitterion was visually compared to the calculated spectra of the different conformers in the LH13C solvation model to determine their agreement. Additional calculations were performed on the LH17 model using increasing basis set functions to investigate the effect of the level of theory used on the theoretical spectra. A spectral analysis was carried out using a set of defined internal coordinates and the potential energy distribution (PED). A theoretical water subtraction was preformed by extracting the coordinates of the histidine molecule from the complete Hessian. The VA spectrum of the isolated LH was recalculated and compared to the experimental spectra.

To study the effect of deuterium substitution the spectra of the LH13C model were recalculated with the different masses. In the first model the deuterium substitution was applied to the solvent molecules only while in the second calculation both the solvent and histidine were subject to substitution. The calculated spectra were analyzed using the PED and compared to the experimental spectra of a LH solution in D_2O.

To confirm the results from the IR analysis using a smaller basis set, the more computationally expensive Raman, VCD and ROA spectra were calculated only for the two lowest energy structures using a larger basis set. These spectra were visually compared to the appropriate experimental spectra. This approach allows the least expensive calculations to be used to draw preliminary conclusions and the more expensive calculations to be used only for confirmation of the results. The sensitivity of VCD and ROA spectroscopies to chirality confers an enhanced sensitivity to the details of the three-dimensional structure (including absolute configuration, and in many cases secondary structure for the peptide and protein backbone, and the side chain dihedral angles for residues like histidine).

2 Materials and methods

2.1 Species distribution plot

The fraction of each of the five protonation states present in solution is mainly a function of pH. In order to characterize the different species by means of vibrational spectroscopy the sample solution should ideally only contain one of the five protonation states. As the species exist in equilibrium it is necessary to identify the pH at which the fractional abundance of a protonation state is as high as possible. Using the reported pK_a values of each species [2] and the equations of the successive equilibria the fraction of a species can be calculated for any given pH. This enables the construction of a plot identifying the distribution (α) of the different species as a function of pH. Such a graph was constructed for each species by solving the corresponding equation for pH intervals of 0.2 between 0 and 14. The plot was used to identify the pH of maximum fraction for each of the protonation states, which were later used to prepare the solution for the IR measurements.

2.2 Chemicals and solutions

DL-histidine was purchased from Sigma Chemicals and used without further purification. The solutions for the IR

Table 1 Nomenclature and initial values of geometrical parameters for the L-histidine zwitterion

Geometry	Naming	χ_2(°)	χ_1(°)
Trans plus	tp	180	90
Trans minus	tm	180	–90
Gauche plus plus	gpp	60	90
Gauche plus minus	gpm	60	–90
Gauche minus plus	gmp	–60	90
Gauche minus minus	gmm	–60	–90
Bond lengths (Å)	O1–C3	1.22	
	O2–C3	1.22	
	C3–C4	1.51	
	C4–N5	1.46	
	C4–C6	1.53	
	C6–C7	1.50	
	C7–N8	1.35	
	C8–N9	1.37	
	N9–C10	1.32	
	C10–N11	1.32	
	N11–C7	1.38	

measurements were freshly prepared at a concentration of 0.10 M for the solution at pH 7.6 and 0.25 M for all other solutions. The pH was measured at room temperature (23°C) with a calibrated Cyberscan-100 pH meter. The solutions were rendered acidic or basic with hydrochloric acid and sodium hydroxide solutions.

The solution for the VCD measurement was prepared at a concentration of 0.3 M at a pH of 7.6

For the Raman and ROA spectra the solution was prepared using LH from Fluka without further purification. It was dissolved in distilled de-ionized water at a concentration of 0.26 M.

2.3 Spectroscopy

The IR measurements were carried out on a Bruker IFS 66 Fourier Transform spectrometer using a DTGS detector and a horizontal ATR accessory with a ZnSe crystal. The sample compartment was flushed with dry air for ~5 min prior to data collection to reduce the interferences of H_2O and CO_2 bands. The spectra were collected using a resolution of 2 cm^{-1} and 256 accumulations. Spectral analysis was carried out after a background subtraction of the water spectrum at the corresponding pH. To compare the experimental spectra to the calculated ones the absorbance units were converted to molar absorptivity. The path-length was determined from a pure water spectrum collected using a transmission cell of known path length.

The VCD spectroscopy measurements were performed on a ChiralIR from BioTools with a 30 um pathlength cell at 8 cm^{-1} resolution over a time of 12 h. Spectral analysis was carried out after a background subtraction of the water spectrum at the corresponding pH.

The Raman and ROA spectra were collected with a BioTools ChiralRAMAN instrument. The details have been reported previously [41,42]. Experimental conditions were: laser wavelength 532 nm, laser power at the sample ~500 mW, resolution ~10 cm^{-1}, acquisition time ~7 h.

All measurements were carried out at room temperature.

2.4 Nomenclature and initial structures

Figure 1 shows the numbering of the atoms in the histidine molecule used throughout the calculations to facilitate comparison of geometrical parameters in the different conformations. The conventional definition of the dihedral angles $\chi_1(N_5–C_4–C_6–C_7)$ and $\chi_2(C_4–C_6–C_7–N_{11})$ are used. χ_1 shows the values trans (180°), gauche minus (−60°) and gauche plus (60°) while χ_2 is either plus (90°) or minus (−90°). The different combinations of χ_1 and χ_2 uniquely define the six geometrical conformations. Table 1 shows the naming of the six conformers as well as their corresponding values of χ_1 and χ_2 and the bond lengths of the starting geometries. Note that due to the presence of the explicit water molecules solvating the polar NH_3^+ and COO^- groups the formation of internal hydrogen bonds is much less likely than in the gas phase. Huang et al. [43] showed that when modeling histidine in the gas phase the internal hydrogen bonding is important as it affects the dihedral angles. Additionally in the gas phase the amino group is NH_2 and the carboxyl group COOH. Here the OH group can H-bond with the lone pair of the nitrogen atom in the imidazole ring. The

hydrogen bonded to the other nitrogen atom in the imidazole ring can H-bond with both oxygens of the COO^- group in the zwitterion, while only with the carboxyl oxygen in the COOH group.

The initial structures of the isolated zwitterion were obtained using the histidine molecule from the amino acid library in the Molden package [44]. The dihedral angles of the six conformers were set to the appropriate values for each conformer as defined in Table 1. For the LHC model the histidine molecule was embedded in a dielectric medium using the COSMO model in ADF [40]. The LH13 model was constructed using the optimized structure of L-alanine solvated with 11 explicit water molecules. This structure was produced in a previous study [45] using MD simulations to determine the optimal position and number of water molecules. The methyl group of L-alanine was replaced by the imidazole ring and additional water molecules were placed close to N_{11} and N_9 to obtain the LH13 and LH17 models. Adding COSMO to LH13 and LH17 resulted in the models LH13C and LH17C.

2.5 Computational methods

The DFT method was employed with the 6-31G(d) and 6-31G(d,p) basis sets in Gaussian 03 and DZP and TZP basis sets in the ADF program for both the geometrical optimisations and the spectral calculations. The exchange and correlation effect are described using the B3LYP hybrid exchange correlation functional in Gaussian and OPBE0 in ADF. The COSMO model in ADF and the PCM in Gaussian use a dielectric constant of 78.39 for water. The main reason for employing the Gaussian program in addition to ADF is that the former allows easy extraction of the Hessian from the output files for off-line processing such as theoretical water subtraction.

The Hessian and atomic polar tensor (APT) calculations were performed on the fully optimized geometry using the numerical Hessian in ADF and Gaussian, as the analytical Hessian is not yet implemented with the continuum model. The VA spectra were related to the molecular dipole strength as described previously [34,46]. The VA spectra were constructed using Lorentzian line shapes with a bandwidth of $8\,cm^{-1}$. The theoretical spectra were not scaled to fit the experimental data as the application of a scaling factor to the force constant matrix means that the results lose some of their predictive potential. The vibrational analysis was carried out within the harmonic oscillator approximation. The Cartesian coordinates obtained from the vibrational frequency calculations were converted into a set of internal coordinates in accordance with those proposed by Pulay et al. [47]. This set was used to construct the corresponding potential energy distribution (PED) to assign the normal modes of the vibrational frequencies. The PED has been used as previously defined by Pulay et al. [47]. The zwitterion solvated with 17 explicit waters constitutes a system of 59 atoms resulting in a set of 171 internal coordinates. To simplify the spectra the modes related to the isolated LH were extracted from the full spectra. The contribution of the solvent molecules in the Hessian was eliminated and the minimised force constant matrix was used to recalculate the frequencies of the isolated LH. These were combined with the corresponding APT to determine the intensities of the VA spectra. It should be noted that this method neglects the direct coupling of the water molecules to the histidine. Thus the full effect of explicit water is present in the optimized structures but not present in the frequency calculations.

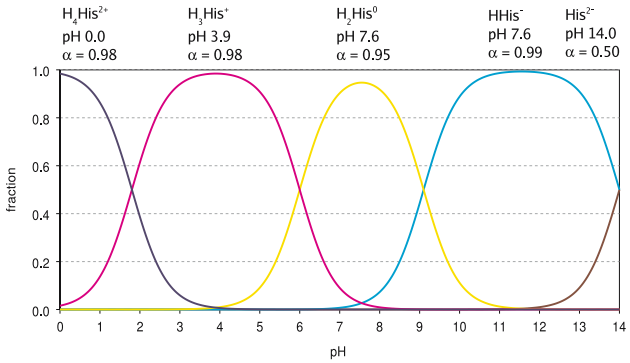

Fig. 2 Fractional distribution (α) of the protonation states of L-histidine in aqueous solutions as a function of pH

3 Results and discussion

3.1 Fraction of histidine species as a function of pH

Figure 2 shows the fraction of each protonation state as a function of pH. It also lists the maximum fraction of each species and the corresponding pH. In acidic solutions both the species $H_4his^{2+}$and H_3his^+ show an abundance of more than 98% at their identified pHs of 0.0 and 3.9. The zwitterion shows as slightly lower abundance of 95% at a pH of 7.6 suggesting an increased competition for protons compared to the acidic and basic solutions. As the pH increases the negatively charged $Hhis^-$ becomes dominant and his^{2-} can only exist in a very basic solution and even at a pH of 14 the fraction is only 0.5. These results suggest that, except for basic solutions above a pH of 12, a solution prepared at one of the identified pHs consists almost solely of one of the five protonation states.

3.2 The effect of different solvation models on the geometrical parameter and relative energies of the optimised conformers

The first set of calculations of the isolated zwitterion showed that, at the B3LYP/6-31G(d) level of theory, the

zwitterion is not stable in the gas phase. During the optimization the proton on the positively charged NH_3^+ group was transferred to the negatively charged COO^- group to form the neutral species. Similar observations have been reported previously for the zwitterion of L-alanine [27], glycine [27] and L-alanyl-L-alanine [31]. These studies found that on the potential energy surface there is no barrier to the proton transfer between the ammonium group to the adjacent carboxylate group. An investigation of the dipeptide L-alanyl-L-alanine showed that by changing from the B3LYP/6-31G(d) to MP2/6-31G level of theory a stable form of the isolated zwitterion could be obtained [31]. These results confirm the need for a careful evaluation of solvation models and level of theory. Additionally the work on the alanine dipeptide showed that even the topology of the potential energy surface can change by including explicit water molecules [25,34], a result which helped clarify and explain contradictory results which previously could not be explained by using only isolated state calculations or implicit solvent models [35]. The results of the isolated histidine in the gas phase were not used for further calculations.

Table 2 shows a summary of the dihedral angles, bond lengths and relative energies obtained from the optimisation of the six conformers in LHC, LH13 and LH13C models. A first inspection of the bond lengths shows that they have not been affected substantially by the optimisation and are independent of the solvation model. The bond lengths show less than 0.10 Å variations before and after the optimisation as well as among the different solvation models. The bond lengths in the imidazole ring are in good agreement with the ones reported in studies for 4-methylimidazole [2,16] and 4-ethylimidazole [18] calculated at the B3LYP/6-31G level of theory.

The results of the COSMO solvation model show that all six conformers retained their initial structure. This indicates that the effect of the bulk water was enough to stabilize the zwitterion. The dihedral angles show deviation from the starting geometry as large as 20°. The changes were especially large for the trans configurations. The lowest energy structure is the gpp conformation. In the LH13 model the dihedral angles of the optimized structures show very different values for all conformers compared to the continuum model. Some angles show differences of more than 30°. Although the gpp structure is still the minimum energy conformation the order of stability has changed. The gmp, which was the least stable structure in the COSMO model, is now the second most stable conformation. The range of relative energies has more than doubled from 17 kJ/mol in the continuum model to 40 kJ/mol in the cluster model. The results from the LH13C model show that in general the addition of a continuum model to a cluster of explicit water does not change the dihedral angles much. Except for the tm structures none of the angles have changed by more than 5°. Despite this, the relative energy of the conformers has been affected substantially by the presence of the reaction field. The order of stability has changed completely with the lowest energy structure now being the gmm conformer. The most stable gpp structure is now the structure of second least stability. This confirms the significant effect solvation has on the geometrical parameters and relative energies of the structure of amino acids reported by other studies [22,23,25,27,29,34,35].

As the choice of solvation model substantially affects the relative energies this parameter should not be used as the single indication of which structure is present in solution but only in addition to other methods such as spectral analyses. Studies on L-alanine [26,27] showed that the number and position of water molecules and the structural parameters and relative energies of the conformers are interrelated. Molecular dynamics simulations can be used to determine the number and position of water molecules in the first hydration shell.

3.3 Spectral analysis: Infrared spectroscopy

3.3.1 Characteristic bands of the five protonation states of L-*histidine*

Table 3 shows the observed infrared absorption frequencies and assignments for the normal modes of the five protonation states of LH at the identified pHs. All the observed bands were in good agreement with the frequencies reported by Mesu et al. [1]. No further attempt has been made to assign these modes. Table 4 lists the characteristic bands for the five protonation states determined from these frequencies. The fully protonated H_4his^{2+} is easily identified by the presence of the strong stretching bands of C=O and C–O(H) at 1,737 and 1,259 cm^{-1}, as these bands are absent in any other ionic state. A further indication is the sharpness of the NH_3^+ antisymmetric bending band at 1,625 cm^{-1}. In the single protonated H_3his^+ the most intense band is the NH_3^+ antisymmetric bending band, which now shows a shoulder caused by the antisymmetric stretching mode of COO^- at 1,610 cm^{-1} . The symmetric stretching mode of the COO^- at 1,402 cm^{-1} is only of medium intensity in this protonation state. In the zwitterion the antisymmetric stretching mode of COO^- at 1610 cm^{-1} has become the most dominant peak with the NH_3^+ bending mode at 1,646 cm^{-1} being the shoulder. The symmetric stretching mode of the COO^- at 1,402 cm^{-1} is stronger than in H_4his^{2+}. The single deprotonated state $HHis^-$ is marked by the disappearance of the shoulder and the shift of the NH_3^+ bending band to 1,562 cm^{-1} . Another indication is the absence of the symmetric bending mode at 1,521 cm^{-1} due to the deprotonation of NH_3^+. The fully deprotonated state his^{2-} is characterised by the absence of the weak band at 1,496 cm^{-1} .

Table 2 Comparison of bond lengths (Å), dihedral angles (°) and energies relative to the lowest energy conformer ΔE (kJ/mole) for the optimized structures (OPBE0/DZP) of the six geometrical conformers of the L-histidine zwitterion in the different solvation models

	tp	tm	gpp	gpm	gmp	gmm
LHC						
O1–C3	1.25	1.25	1.25	1.25	1.24	1.26
O2–C3	1.27	1.27	1.26	1.27	1.27	1.25
C3–C4	1.56	1.56	1.55	1.56	1.56	1.56
C4–N5	1.48	1.49	1.48	1.48	1.48	1.48
C4–C6	1.53	1.53	1.52	1.52	1.52	1.52
C6–C7	1.48	1.48	1.49	1.49	1.49	1.49
C7–N8	1.37	1.37	1.38	1.38	1.37	1.38
C8–N9	1.37	1.37	1.37	1.37	1.37	1.37
N9–C10	1.32	1.32	1.32	1.32	1.32	1.32
C10–N11	1.35	1.35	1.35	1.35	1.35	1.35
N11–C7	1.37	1.37	1.37	1.38	1.37	1.37
χ_1	−165.96	−170.38	59.26	60.30	−65.11	−60.85
χ_2	70.27	−97.93	88.54	−93.15	76.73	−82.89
Δ E	8.61	6.14	0.00	7.98	17.01	7.48
LH13						
O1–C3	1.24	1.24	1.25	1.24	1.24	1.24
O2–C3	1.26	1.26	1.26	1.26	1.26	1.26
C3–C4	1.56	1.56	1.56	1.56	1.56	1.56
C4–N5	1.48	1.48	1.48	1.48	1.48	1.48
C4–C6	1.53	1.52	1.53	1.52	1.52	1.52
C6–C7	1.49	1.49	1.48	1.49	1.49	1.48
C7–N8	1.37	1.38	1.37	1.37	1.37	1.37
C8–N9	1.36	1.37	1.37	1.37	1.36	1.37
N9–C10	1.32	1.32	1.32	1.31	1.31	1.31
C10–N11	1.35	1.35	1.35	1.35	1.35	1.35
N11–C7	1.37	1.37	1.37	1.38	1.37	1.37
χ_1	−170.22	−162.39	58.86	59.95	−69.09	−66.54
χ_2	76.49	−101.97	79.50	−94.53	103.97	−74.01
Δ E	32.61	4.17	0.00	40.49	3.18	5.07
LH13C						
O1–C3	1.24	1.24	1.25	1.25	1.25	1.24
O2–C3	1.26	1.27	1.26	1.26	1.26	1.27
C3–C4	1.55	1.55	1.55	1.55	1.55	1.55
C4–N5	1.48	1.48	1.48	1.48	1.48	1.48
C4–C6	1.53	1.53	1.52	1.52	1.52	1.52
C6–C7	1.48	1.49	1.49	1.49	1.49	1.48
C7–N8	1.37	1.37	1.37	1.37	1.37	1.37
C8–N9	1.36	1.37	1.37	1.37	1.37	1.37
N9–C10	1.32	1.32	1.32	1.32	1.32	1.32
C10–N11	1.35	1.34	1.35	1.35	1.35	1.35
N11–C7	1.37	1.37	1.37	1.37	1.37	1.37
χ_1	−167.95	−163.15	54.50	63.91	−69.35	−63.32
χ_2	72.66	−113.41	81.88	−91.84	105.18	−75.89
ΔE	19.72	14.89	32.37	35.50	13.05	0.00

Table 3 Observed infrared absorption frequencies (cm^{-1}) and assignments of the five protonation states of L-histidine in aqueous solutions at specific pHs

H_4His^{2+} pH0.0	H_3His^{+} pH3.9	H_2His^{0} pH7.6	$HHis^{-}$ pH 11.4	His^{2-} pH 14.0	Assignment [1]
1,737	–	–	–	–	νC=O
1,625	1,623	1,646 (sh)	–	–	$\delta_{as}NH_3^+$
–	1,610 (sh)	1,600	1,562	1,558	$\nu_{as}COO^-$
1,535	1,525	1,521	–	–	νRing /$\delta_s NH_3^+$
–	–	1,500 (sh)	1,493	–	δN–H i.p. / ν C=N
1,439	1,438	1,438	1,436	1,436	δCH_2
–	1,402	1,409	1,410	1,419	$\nu_s COO^-$
1,365	1,361 (sh)	1,355	1,355	1,355	δCH_2 wagging
–	1,347	1,346	–	–	βNH_3^+
1,296 (sh)	1,297	–	–	–	νC–N + δ=C–H
–	–	1,285	1,288	1,287	ν= C–N + δC–H
–	1,266	1,265	1,263	–	ν= C–N + δC–H
1,259	–	–	–	–	ν_sC–O
1,242 (sh)	1,242	1,223	1,230	1,230	ν C–N + C–C +δC–H
1,190 (sh)	1,185	1,193	1,199	1,199 (sh)	δ – C–H(γCH_2)
1,161	1,149	1,139	1,155	1,152	ν=C–N /δ=N–H
–		1,106	1,104	1,104	ν = C–N/δ = C–H(N^{π})
1,095	1,093	1,091	1,087	1,088	ν = C–N/δ = C–H(N^{τ})
1,069 (sh)	1,054	1,051	1,022	1,010	ν=C–N side chain
992	991	990	988	–	ν=C–N /δ ring
970	970	962	–	–	δNH_3^+
–	–	939	940	939	δRing
916	919	916	–	–	δC–H i.p.

3.3.2 *Effect of different solvation models on the theoretical spectra of the* L-*histidine zwitterion*

The VA spectra of the LH zwitterion calculated with the five different solvation models in comparison to the experimental spectra are shown in Fig. 3. A visual comparison of all the spectra shows that overall the regions between 1,400 – 1,700 cm^{-1} and above 2,800 cm^{-1} are affected the most by the change in solvation model. These regions correspond to the bands of the functional groups COO^- and NH_3^+. The polar nature of these groups explains why the addition of both explicit water and a dielectric medium will show more effect in these areas of the spectra than in regions corresponding to modes of the non-polar regions of the molecule. Both COO^- and NH_3^+ show strong interactions with water and build the main connection between LH and the cluster of solvent molecules.

Comparing the spectra of the LHC and LH13 models shows that adding explicit water molecules causes the appearance of many new bands in the amide A region ($\sim$ 3,300 cm^{-1}) and doubles the intensity of these bands. This results in a spectrum that shows a much better visual agreement with the experimental one than the LHC model. The carboxylate area around 1,600 cm^{-1} shows additional bands which results in a pattern that resembles more the observed bands in the experimental spectrum. The intensity of these bands is not increased which causes the intensity ratio of the carboxylate and amide A region to be very different to the LHC model. A comparison of the LH13 and LH17 spectra shows that the major effect of adding more explicit water molecules to the model is an increase in intensity in the region above 3,000 cm^{-1}, which further distorts the intensity ratio between the carboxylate and amide region. A closer inspection indicates that the bands in both these areas are shifted. To visualize the effect of adding the continuum model to the explicit solvent molecules Fig. 4 shows the overlay of the LH13/LH13C and LH17/LH17C spectra. This comparison shows the appearance of additional bands in the amide A region which together with an increase in intensities gives the impression of broader bands. The addition of the continuum

Table 4 Characteristic IR bands for the five protonation states of L-histidine observed at specific pHs

H_4His^{2+} pH 0.0	H_3His^{+} pH 3.9	H_2His^{0} pH 7.6	$HHis^{-}$ pH 11.4	His^{2-} pH 14.0	Assignment [1]
1,737	–	–	–	–	νC=O
1,625	1,623	1,646 (sh)	–	–	$\delta_{as}NH_3^+$
–	1,610 (sh)	1,600	1,562	1,558	$\nu_{as}COO^-$
1,535	1,525	1,521	–	–	$\delta_sNH_3^+$
–	–	1,500 (sh)	1,493	–	δN–H i.p./ν C=N
–	1,402	1,409	1,410	1,419	ν_sCOO^-
–	1,266	1,265	1,263	–	ν=C–N + δC–H
1,259	–	–	–	–	ν_sC–O

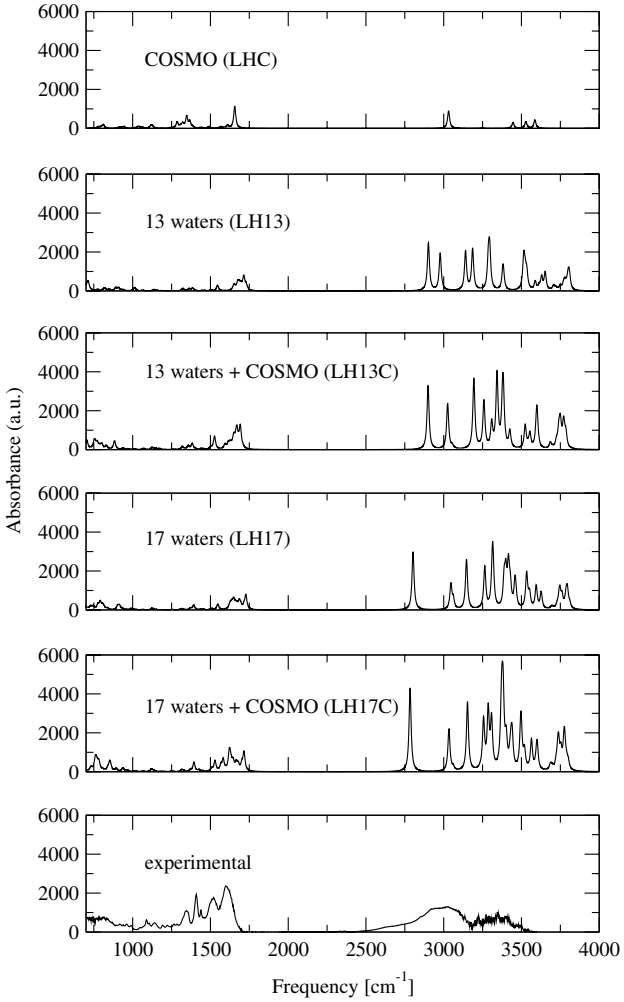

Fig. 3 Vibrational absorption spectra of the L-histidine zwitterion (tm conformer) calculated at the 6-31G(d,p) level in the different solvation models in comparison to the experimental spectrum of a L-histidine solution at pH 7.6

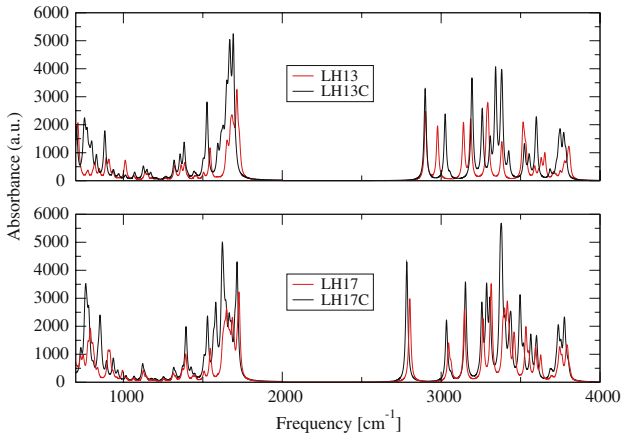

Fig. 4 Effect of adding a dielectric continuum model to explicit solvent molecules on the calculated spectra of the L-histidine zwitterion

model causes the bands below 2,000 cm^{-1} to be shifted to lower frequency while the peaks above 3,000 cm^{-1} experience a shift to higher frequency. The shifts of these bands in combination with the broadening effect result in a better visual agreement with the experimental spectrum. A more detailed study of the effect of the solvation model on the spectra of LH could be achieved by means of an assignment of the individual bands using a set of internal coordinates and PEDs.

The comparison of the spectra confirms the results of previous studies that the combination of explicit solvent molecules with a continuum model shows the best agreement with experimental spectra indicating that the combination of these solvation models is the best representation of the real system. It should be noted that the addition of explicit solvent molecules causes a substantial increase in the cost of computation for the calculation of the spectra. It is advisable to invest some effort in molecular dynamics (MD) simulations to determine the number and position of the solvent molecules in the first hydration shell. The computational effort for the calculations of the spectra can then be applied to the optimised structure of the minimum energy conformation.

3.3.3 *The effect of changes in the basis set on the calculated spectra*

Figure 5 shows the effect of expanding the basis set on the calculated spectra of the LH zwitterion. Similar to the effect of the choice of solvation model the bands in the carboxylate (1,400–1,700 cm^{-1}) and amide A region (above 3,000 cm^{-1}) are affected more than skeleton regions. Again this reflects the polar nature of these functional groups as an increase in the basis set corresponds to the addition of polarizability and a better description of the electronic structure. The two regions show a similar shift of frequencies as described in Sect. 3.3.2, resulting in a better agreement with the experimental spectrum with increasing basis set. The intensities of the amide A region and the skeleton bands below 1,000 cm^{-1} are lowered with increasing basis set while the overall level of intensity of the bands in the carboxyl area is unchanged. As a consequence the relative intensity of these two regions shows a better resemblance to the experimental spectrum.

3.3.4 *Comparison of the theoretical spectra of different conformations of zwitterion to the experimental spectra*

Using the VA spectra to assist in the determination of the species present in solution requires the conformers to be distinguishable by their spectra. Figure 6 shows the calculated spectra of the six conformers of the LH zwitterion in the LHC solvation model. The first characteristic feature that can be used to differentiate is the position of the strong peak at ~1,650 cm^{-1}. The pattern of position and relative intensities of the bands in the 1,300–1,400 cm^{-1} region are another source of discrimination. A combination of these two areas makes it possible to uniquely identify the conformer present. These features are still present in the more complex LH13C spectra and can be used when comparing the calculated spectra of the different conformers to the experimental spectrum (Fig. 7). In addition the pattern of peaks below 1,000 cm^{-1} is another characteristic that is useful for ruling out some of the conformers. The LH13C model has been chosen for comparison as this is an acceptable compromise between a good solvation model and computational cost. Using the three areas of characteristic features, the gmm conformer shows the best agreement with the experimental spectrum followed by the gmp conformer. This confirms the results from the structural optimisation that predicted the gmm conformer to be the lowest energy structure. It should be noted that the actual solution might be a mixture of different conformations. To assess this, a more detailed analysis of the conformers and their characteristic bands by numerical comparison of the frequencies and intensities of the experimental spectrum to the modes identified by a PED assignment as demonstrated

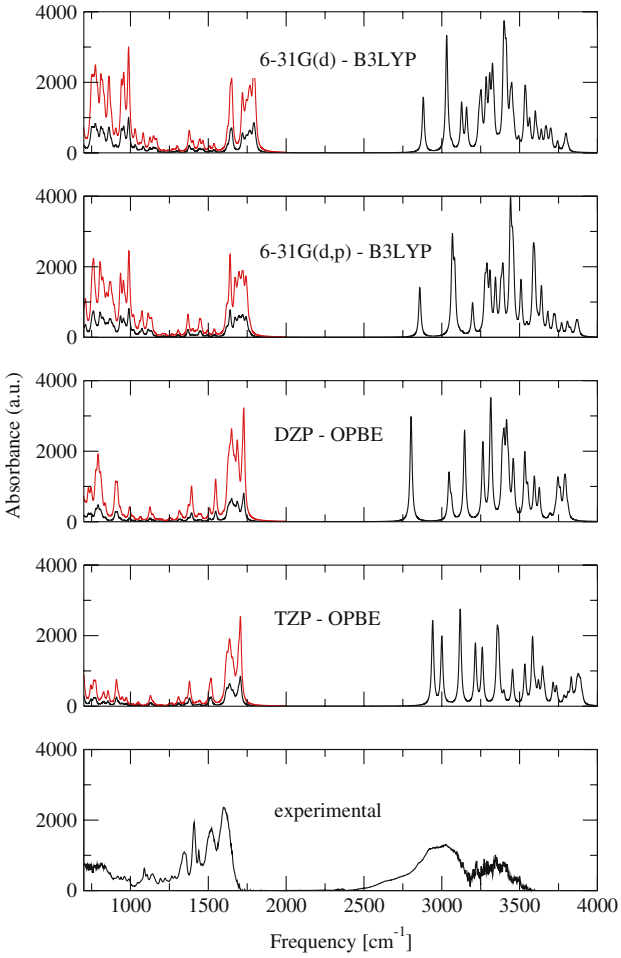

Fig. 5 Vibrational absorption spectra of the L-histidine zwitterion solvated with 17 explicit water molecules calculated using different basis sets. The region between 700–2000 cm^{-1} has been scaled by 3.0. Experimental spectrum of a L-histidine solution at pH 7.6

for the structures of L-alanine in ref. [27] may be useful. The use of a VCD and ROA spectra might also provide additional information in the discrimination of the conformers and the determination of the structure present in solution.

3.3.5 *Theoretical water subtraction of calculated spectra*

Although the use of a solvation model that considers both bulk and explicit solvent interactions substantially increases the agreement of the calculated spectrum to the experimental one, it makes the assignment of the modes more complex due the larger number of bands present. To facilitate the assignment of the modes of the LH molecule its Hessian has been extracted from the complete force constant matrix and the frequencies and intensities of the isolated LH recalculated. This minimized set of Cartesian coordinates was converted to internal coordinates according to the method

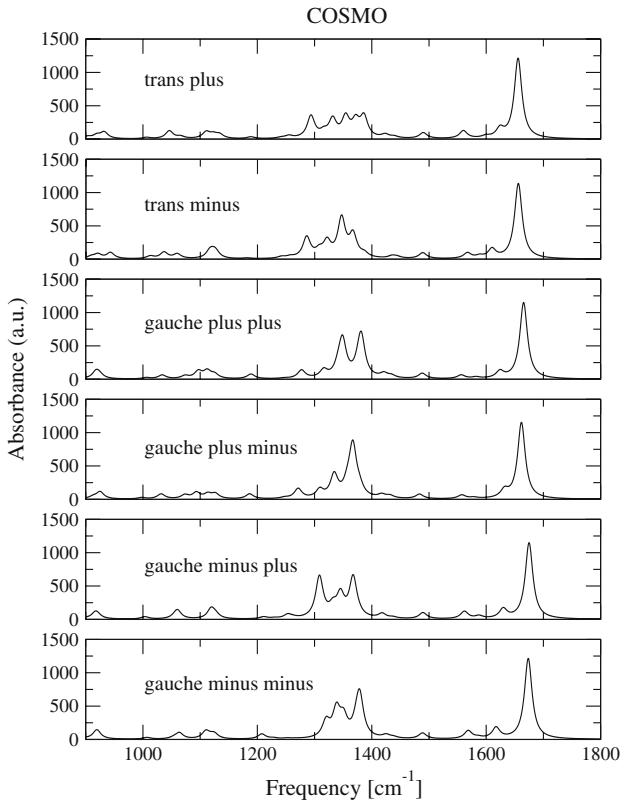

Fig. 6 Vibrational absorption spectra of the six geometrical conformers of the L-histidine zwitterion solvated with the COSMO continuum model calculated at the OPBE0/DZP level

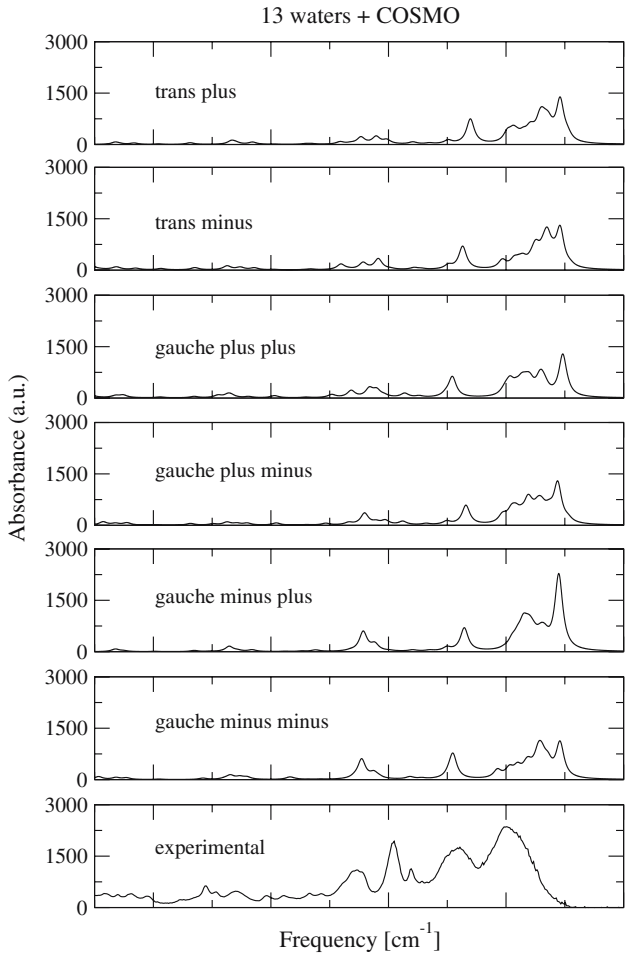

Fig. 7 Vibrational absorption spectra of the six geometrical conformers of the L-histidine zwitterion solvated with 13 explicit water molecules plus COSMO calculated at the OPBE0/DZP level in comparison to the experimental spectrum of a L-histidine solution at pH 7.6

described by Pulay et al. [47]. Table 5 shows the internal coordinates defined for the LH zwitterion. They agree with the set defined for 4-methylimidazole reported by Majoube et al. [17]. Figure 8 shows the calculated spectra for the two low energy conformers gmm and gmp before and after the theoretical water subtraction compared to the experimental spectrum. Table 6 lists the observed and calculated frequencies and assignments for the normal modes of the gmm and gmp conformers together with the data from the experimental spectrum. A visual comparison of the before and after spectra of both conformers shows that the areas most affected by the water subtraction are the amide A region and the bands below 1,000 cm^{-1}. The elimination of the bulk water from the amide A region reduces the previously large number of peaks, which allows the easier assignment of these bands. According to the PED these bands can be assigned to the stretching modes of the NH_3^+, COO^- and the C–H stretches of the backbone and the imidazole ring. The number of bands in the region below 1,000 cm^{-1} is also substantially reduced by the subtraction of the water. The PED shows that the bands in this area are mainly due to deformations of the backbone. The COO^- bands around 1,600 cm^{-1} is another region that is simplified by the water subtraction. As the bands in these two regions can be used to discriminate the different conformers this simplification enables the identification of characteristic bands. Theoretically the bands in the amide region might be an additional source for differentiation but these bands are buried under broad water peaks in the experimental spectrum, limiting their practical use. A comparison of the frequencies of the gmp and gmm conformers in Table 6 confirms the use of the COO^- and NH_3^+ bands in the 1,600–1,700 cm^{-1} and the pattern of the bands in the 1,300–1,400 cm^{-1} regions for the discrimination of the conformers. A comparison of the frequencies to the experimental spectrum in these regions confirms gmm being the conformer with the best agreement as determined from the visual comparison in Sect. 3.3.4.

Figure 8 also shows that the region above 3,000 cm^{-1} in the calculated spectra is very different to the experimental spectrum. This reflects the difference of how the water subtraction is performed in the experimental and the calculated spectra. In the case of an experimental spectrum the back-

Table 5 Internal coordinates of the L-histidine zwitterion extracted from the LH17 B3LYP/6-31G(d,p)calculations

No	Mode	Description
q_1	R_1	N_5–H_{18} stretch
q_2	R_2	N_5–H_{19} stretch
q_3	R_3	N_5–H_{20} stretch
q_4	R_4	C_6–H_{15} stretch
q_5	R_5	C_6–H_{16} stretch
q_6	R_6	C_7–C_6 stretch
q_7	R_7	C_4–H_{17} stretch
q_8	R_8	O_2–C_3 stretch
q_9	R_9	O_1–C_3 stretch
q_{10}	R_{10}	C_4–N_5 stretch
q_{11}	R_{11}	C_4–C_3 stretch
q_{12}	R_{12}	C_4–C_6 stretch
q_{13}	$(\alpha_1+\alpha_2+\alpha_3-\beta_1-\beta_2-\beta_3)/\sqrt{6}$	Sym NH_3^+ deformation
q_{14}	$(2\alpha_1-\alpha_2-\alpha_3)/\sqrt{6}$	Asym NH_3^+ deformation
q_{15}	$(\alpha_2-\alpha_3)/\sqrt{2}$	Asym NH_3^+ deformation
q_{16}	$(2\beta_1-\beta_2-\beta_3)/\sqrt{6}$	C–N–H rocking
q_{17}	$(\beta_2-\beta_3)/\sqrt{2}$	C–N–H rocking
q_{18}	$(\beta_1^{i}-\beta_2^{i}+\beta_3^{i}-\beta_4^{i})/\sqrt{4}$	CH_2 rocking
q_{19}	$(\beta_1^{i}+\beta_2^{i}-\beta_3^{i}-\beta_4^{i})/\sqrt{4}$	CH_2 wagging
q_{20}	$(\beta_1^{i}-\beta_2^{i}+\beta_3^{i}+\beta_4^{i})/\sqrt{4}$	CH_2 twisting
q_{21}	$(5\alpha^{ii}+\gamma^{ii})/\sqrt{26}$	CH_2 scissoring
q_{22}	$(\alpha^{ii}+5\gamma^{ii})/\sqrt{26}$	C–C–C scissoring
q_{23}	$(2\beta_1^{iii}-\beta_2^{iii}-\beta_3^{iii})/\sqrt{6}$	CH rocking
q_{24}	$(\beta_2''-\beta_3'')/\sqrt{2}$	CH rocking
q_{25}	$(4\alpha_{YCZ}+\alpha_{XCZ}+\alpha_{XCY})/\sqrt{18}$	YCZ deformation
q_{26}	$(4\alpha_{XCZ}+\alpha_{YCZ}+\alpha_{XCY})/\sqrt{18}$	XCZ deformation
q_{27}	$(4\alpha_{XCY}+\alpha_{YCZ}+\alpha_{XCZ})/\sqrt{18}$	XCY deformation
q_{28}	$(2\alpha^{iv}-\beta_1^{iv}-\beta_2^{iv})/\sqrt{6}$	Sym COO deformation
q_{29}	$(\beta_1^{iv}-\beta_2^{iv})/\sqrt{2}$	COO rocking
q_{30}	R_{30}	C_4–C_3 oop
q_{31}	R_{31}	H_{18}–N_5–C_4–C_3 torsion
q_{32}	R_{32}	H_{15}–C_6–C_4–N_5 torsion
q_{33}	R_{33}	N_5–C_4–C_3–O_2 torsion
q_{34}	R_{34}	C_7–C_8 stretch
q_{35}	R_{35}	C_7–N_{11} stretch
q_{36}	R_{36}	C_8–N_9 stretch
q_{37}	R_{37}	N_{11}–C_{10} stretch
q_{38}	R_{38}	C_8–H_{14} stretch
q_{39}	R_{39}	C_{10}–H_{13} stretch
q_{40}	R_{40}	N_{11}–H_{13} stretch
q_{41}	R_{41}	N_9–C_{10} stretch
q_{42}	$(\beta_1^{v}-\beta_2^{v})/\sqrt{2}$	ip wagging
q_{43}	R_{43}	C_7–C_6 oop wagging
q_{44}	$(\beta_1^{vi}-\beta_2^{vi})/\sqrt{2}$	ip wagging
q_{45}	R_{45}	C_8–H_{14} oop wagging
q_{46}	$(\beta_1^{vii}-\beta_2^{vii})/\sqrt{2}$	ip wagging
q_{47}	R_{47}	C_{10}–H_{13} oop wagging
q_{48}	$(\beta_1^{viii}-\beta_2^{viii})/\sqrt{2}$	ip wagging
q_{49}	R_{49}	N_{11}–H_{12} oop wagging
q_{50}	$(\alpha_1^{ix}+a(\alpha_2^{ix}+\alpha_5^{ix})+b(\alpha_3^{ix}+\alpha_4^{ix}))/\sqrt{3.39}$	Ring deformation

Table 5 continued

No	Mode	Description
q_{51}	$((a-b)(\alpha_2^{ix}-\alpha_5^{ix})+b(\alpha_3^{ix}+\alpha_4^{ix}))/\sqrt{8.63}$	Ring deformation
q_{52}	$b(\tau_1^{ix}+\tau_5^{ix})+a(\tau_2^{ix}+\tau_4^{ix})+\tau_3^{ix})/\sqrt{3.39}$	Ring torsion
q_{53}	$((a-b)(\tau_4^{ix}+\tau_2^{ix})+(1-a)(\tau_5^{ix}+\tau_1^{ix}))/\sqrt{6.79}$	Ring torsion
q_{54}	τ_6^{ix}	Side chain torsion

$\alpha_1 = H_{18}–N_5–H_{20}, \alpha_2 = H_{18}–N_5–H_{19}, \alpha_3 = H_{19}–N_5–H_{20}$
$\beta_1 = H_{19}–N_5–C_4, \beta_2 = H_{20}–N_5–C_4, \beta_3 = H_{18}–N_5–C_4$
$\beta_1^{i} = H_{15}–C_6–C_4, \beta_2^{i} = H_{16}–C_6–C_4, \beta_3^{i} = H_{15}–C_6–C_7, \beta_4^{i} = H_{16}–C_6–C_7$
$\alpha^{ii} = H_{15}–C_6–H_{16}, \gamma^{ii} = C_7–C_6–C_4, \beta_1^{iii} = H_{17}–C_4–N_5, \beta_2^{iii} = H_{17}–C_4–C_3, \beta_3^{iii} = H_{17}–C_4–C_6$
$\alpha_{XCY} = C_6–C_4–N_5, \alpha_{XCZ} = C_6–C_4–C_3, \alpha_{YCZ} = N_5–C_4–C_3, \alpha^{iv} = O_2–C_3–O_1$
$\beta_1^{iv} = C_4–C_3–O_2, \beta_2^{iv} = C_4–C_3–O_1, \beta_1^{v} = C_6–C_7–C_8, \beta_2^{v} = C_6–C_7–N_{11}$
$\beta_1^{vi} = H_{14}–C_8–C_7, \beta_2^{vi} = H_{14}–C_8–N_9, \beta_1^{vii} = H_{13}–C_{10}–C_9, \beta_2^{vii} = H_{13}–C_{10}–N_{11}$
$\beta_1^{viii} = H_{12}–N_{11}–C_{10}, \beta_2^{viii} = H_{12}–N_{11}–C_7$
$\alpha_1^{ix} = N_{11}–C_7–C_8, \alpha_2^{ix} = C_7–N_{11}–C_{10}, \alpha_3^{ix} = N_{11}–C_{10}–C_9, \alpha_4^{ix} = C_8–N_9–C_{10}$
$\alpha_5^{ix} = N_9–C_8–C_7$
$\tau_1^{ix} = C_7–N_{11}, \tau_2^{ix} = N_{11}–C_{10}, \tau_3^{ix} = C_{10}–N_9, \tau_4^{ix} = N_9–C_8, \tau_5^{ix} = C_8–C_7, \tau_6^{ix} = C_6–C_7$
$a = \cos 144°, b = \cos 72°$
oop = out of plane, *ip* = in plane

ground measurement of the solvent is used for the subtraction and therefore only the effect of the bulk water is considered in the subtraction. The final spectrum still contains the contributions of the direct coupling of the solvent molecules to LH. In addition to that, it is likely that in solution at room temperature there exists a number of local minimum for the positions of the solvent molecules coupled to the LH which causes the broadening effects for the bands of the experimental spectrum in this region. In the case of the theoretical water subtraction any contribution from the solvent is removed leaving only the modes caused by the isolated LH. Due to this fundamental difference the spectra look inherently different in the regions where bulk water is known to make a large contribution to the absorption spectra. As the spectrum is calculated in the presence of a solvent model a comparison of the spectrum after subtraction to the spectrum in the LHC model could reveal the perturbation of the amide bands by the presence of explicit water molecules. The definition of a set of internal coordinates for the entire system including the explicit water, as reported by Frimand et al. for L-alanine [26], would allow a more detailed investigation of the coupling modes and their dependence on the geometrical parameters of the conformer.

3.3.6 The effect of deuterium substitution on the calculated and experimental spectra

The dissolution of histidine in D_2O causes the hydrogens in the NH_3^+ group (H18, H19, H20) and the proton connected to the nitrogen in the imidazole ring (H12) to be substituted by deuterium. In combination with the effect of the substitution in the bulk solvent these alterations substantially change the spectra of the LH zwitterion in solution. Figure 9 shows the experimental spectra of a LH solution at pH(D) of 7.6 in H_2O and D_2O. Note that the broad bands of 3,000–3,500 cm^{-1} in the D_2O spectrum are most likely caused by HDO/H_2O contamination and are ignored in the spectral analysis. The corresponding theoretical spectrum has been calculated using the gmm conformer in the LH13C model. The results have been subjected to the same theoretical solvent subtraction as described in Sect. 3.3.5 to facilitate a numerical comparison of the H_2O and D_2O spectra. Table 7 lists the frequencies of the normal modes for the gmm conformer calculated at the 6-31G(d,p) level in the LH13C model in water and deuterium. A visual comparison of the spectra in Fig. 9 shows that the region between 1,700 and 1,300 cm^{-1} and the bands above 3,000 cm^{-1} are affected the most by deuterium substitution. These are the regions where the bands of bulk solvent as well as the modes of solvent-histidine interactions are positioned. The two intense peaks at 1,600 cm^{-1} and 1,409 cm^{-1} corresponding to the symmetric and antisymmetric modes of the COO^- group seem to be unaffected by the substitution. This is confirmed by the PED analysis (Table 7) which shows that the frequencies of the corresponding modes (q8, q9) only experience a shift of $\sim$10 cm^{-1} . The major changes seem to be caused by the shift of the NH_3^+ modes. Figure 9 shows that the antisymmetric and symmetric deformations of the NH_3^+ group at 1,646 and 1,521 cm^{-1} are shifted towards lower frequencies. This is confirmed by the PED assignment of these modes in Table 7 (q13, q14, q15) which predicts a shift of $\sim$ 450 cm^{-1} down to the 1,200 cm^{-1} region. According to the PED assignment the N–H stretches, buried in the broad water bands in the amide A region, have also been shifted down. The PED also indicates that the stretches and bends in the backbone and side chain skeleton are not much affected by the substitution. The only one of these that is shifted to lower

Table 6 Observed and calculated wavenumbers for the vibrational modes of different conformers of the L-histidine zwitterion

Assignment[a]$_{exp}$	$\nu_{observed}$	$\nu_{calculated}$[c]	Assignment[b]$_{PED}$	$\nu_{calculated}$[d]	Assignment[b]$_{PED}$
		3,381	q40 0.99	3,201	q39 0.55 q8 0.42
		3,247	q2 0.99	3,198	q38 0.56 q39 0.42
		3,206	q38 0.92	3,166	q40 0.95
		3,200	q39 0.92	3,135	q3 0.94
		3,125	q4 0.53 q5 0.44	3,117	q5 0.62 q4 0.35
		3,084	q7 0.83 q5 0.14	3,069	q4 0.57 q5 0.36
		3,075	q4 0.45 q5 0.41 q7 0.13	3,054	q7 0.88
		2,961	q3 0.98	3,020	q2 0.95
		2,896	q1 0.99	2,950	q1 0.95
$\delta_{as}NH_3^+$	1,646	1,709	q14 0.81 q16 0.11	1,738	q15 0.65 q14 0.25
		1,700	q15 0.81 q17 0.14	1,701	q14 0.60 q15 0.22 q16 0.10
$\nu_{as}COO^-$	1,600	1,646	q9 0.40 q8 0.25 q13 0.19	1,652	q9 0.41 q8 0.29 q13 0.17
		1,633	q34 0.38 q48 0.19 q6 0.14	1,640	q48 0.35 q34 0.28 q6 0.10
$\delta_sNH_3^+$	1,521	1,623	q13 0.63 q9 0.17	1,622	q13 0.72 q9 0.12
ν C=N	1,500	1,523	q41 0.33 q46 0.26 q37 0.18	1,520	q37 0.26 q41 0.21 q46 0.16 q48 0.16
νRing	1,521			1,513	q34 0.30 q48 0.16 q46 0.10
δCH_2 wagging	1,438	1,498	q21 0.68	1,492	q21 0.76
δN-H i.p.	1,500	1,477	q48 0.28 q21 0.20 q34 0.16 q37 0.11		
ν_sCOO^-	1,409	1,437	q23 0.20 q8 0.20 q11 0.17	1,442	q23 0.31 q8 0.17 q11 0.13
		1,402	q23 0.30 q8 0.15 q17 0.10 q9 0.10	1,408	q23 0.21 q8 0.19 q9 0.13
		1,398	q41 0.20 q35 0.17 q20 0.15	1,414	q35 0.16 q19 0.15 q20 0.13 q6 0.12 q41 0.11
δCH_2 wagging	1,355	1,387	q19 0.40	1,368	q19 0.35 q41 0.10
βNH_3^+	1,346	1,314	q20 0.30	1,323	q20 0.26 q16 0.13
		1,303	q24 0.31 q16 0.17 q44 0.11	1,295	q24 0.21 q44 0.15 q16 0.14 q36 0.14
νC–N + C–C +δC–H	1,223	1,282	q44 0.32 q19 0.12	1,290	q46 0.15 41 0.13 q37 0.12 q44 0.12 q24 0.11
		1,270	q36 0.20 q46 0.11 q35 0.11	1,275	q19 0.24 q36 0.21 q35 0.10
ν = C–N + δC–H	1,285	1,240	q17 0.37 q24 0.15 q16 0.15 q23 0.12	1,197	q17 0.26 q24 0.21
δ–C–H(γCH_2)	1,193	1,178	q37 0.36 q48 0.19 q46 0.13	1,199	q37 0.32 q46 0.18 q17 0.14
ν = C–N /δ = N–H	1,139	1,151	q20 0.29 q16 0.14 q24 0.11 q23 0.11	1,164	q20 0.36 q23 0.15
ν = C–N/δ = C–H(N^{π})	1,106	1,137	q36 0.48 q44 0.20	1,140	q36 0.48 q44 0.22
ν = C–N/δ = C–H(N^{τ})	1,091	1,099	q10 0.40 q12 0.23	1,098	q10 0.34 q12 0.20
ν = C–N side chain	1,051	1,027	q50 0.29 q35 0.12 q34 0.11	1,018	q50 0.36 q35 0.17 q6 0.10 q34 0.10
δ Ring	990	979	q18 0.21 q12 0.15 q27 0.12		
ν = C–N	990			991	q12 0.22 q18 0.26 q27 0.14
δRing	939	949	q51 0.80	950	q51 0.83
δNH_3^+	962	944	q11 0.30 q25 0.11	934	q11 0.27 q18 0.11
δC–H i.p.	916	874	q53 0.42 q49 0.37 q52 0.12	916	q49 0.45 q53 0.35 q52 0.15
		862	q18 0.26 q10 0.17	861	q18 0.27 q10 0.15 q45 0.10
		828	q45 0.35 q52 0.28 q47 0.28	833	q45 0.53 q52 0.19
		821	q47 0.45 q45 0.21	821	q47 0.73
		808	q28 0.21 q45 0.13 q30 0.12	807	q28 0.19 q30 0.16 q26 0.11
		719	q22 0.20 q30 0.19 q43 0.16	716	q22 0.22 q43 0.20 q30 0.19

[a] Assignment of observed wavenumbers according to [13]
[b] Assignment of normal modes on PED according to internal coordinates defined in Table 5 followed by the % contribution. Only contributions larger than 0.1 are considered
[c] gmm conformer
[d] gmp conformer

frequency is the N-H bend of the imidazole ring due to the exchange of H12. This is not visible in the spectrum as this band is of low intensity and buried among the other skeleton stretches in the region below 1,000 cm^{-1} . The other clearly visible change in the experimental spectrum is the shift of the bands of the bulk solvent. Upon deuterium substitution the broad bands around 3,000 cm^{-1} are shifted by ~500 cm^{-1} to the low frequency side clearing the amide A region. The PED assignment of the calculated and water subtracted spectra in Fig. 8 showed that the N–H stretches are usually found in this region. An alternative way to theoretical water subtraction for isolating these bands and confirming their assignment is to calculate the spectra with only substitution of the hydrogens in the solvent but not in the LH molecules. Figure 10 shows the effect of this substitution in comparison to the normal H_2O and D_2O spectra. A comparison of these bands after a theoretical water subtraction in the calculated H_2O and D_2O (Fig. 11) shows that the pattern is not substantially affected by the substitution of the solvent. These spectra demonstrate that deuterium substitution provides an additional method of analysing the individual modes and a confirmation of their assignment.

3.4 Spectral analysis: Raman, VCD and ROA spectroscopy

A first spectral analysis using the IR spectra identified characteristic bands of the six conformers of the zwitterion and, based on the best matching spectra, suggested that the gmm and gmp are the dominant species in solutions. To confirm these results and to test if the species in solution could be assigned to one of the two conformers the Raman (Figs. 12 and 13), VCD (Fig. 14) and ROA (Figs. 15, 16, 17, 18,19, 20) spectra of these two low energy structures were calculated and visually compared to the corresponding experimental spectrum.

3.4.1 Raman spectroscopy

All calculated Raman spectra have been subject to a theoretical water subtraction as described in Sect. 2.5. Figure 12 shows the theoretical Raman spectra of the gmm and gmp conformers, calculated at the B3PW91/6-31G(d) level, in comparison to the experimental spectrum. The two structures show characteristic bands that allow them to be differentiated easily. The most distinctive bands are the two intense peaks for the gmm conformer at 800–900 cm^{-1} which are missing for the gmp structure. Another source of discrimination is the intensity pattern of two peaks in the 1,400–1,500 cm^{-1} region. The gmm also shows two peaks above 1,600 cm^{-1} while the gmp only has one. A first comparison of the experimental spectrum to the calculated ones shows unsatisfactory agreement. The experimental spectrum exhibits a larger number of medium to strong peaks above 1,200 cm^{-1} and

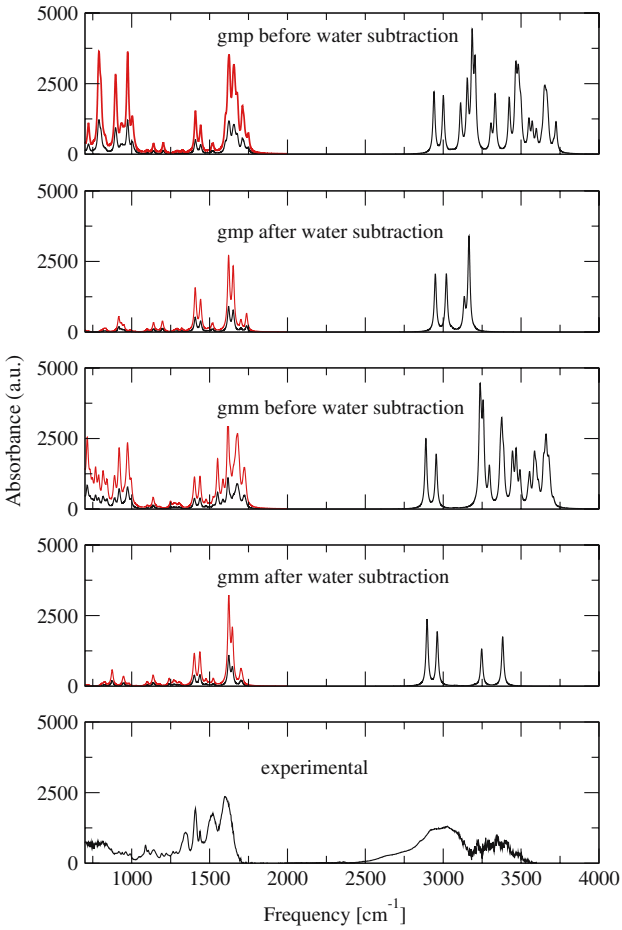

Fig. 8 Vibrational absorption spectra of the L-histidine zwitterion solvated with 13 explicit water molecules plus PCM continuum model calculated at the 6-31G(d,p) level before and after a theoretical water subtraction. The region between 700–2,000 cm^{-1} has been scaled by 3.0. Experimental spectrum of a L-histidine solution at pH 7.6

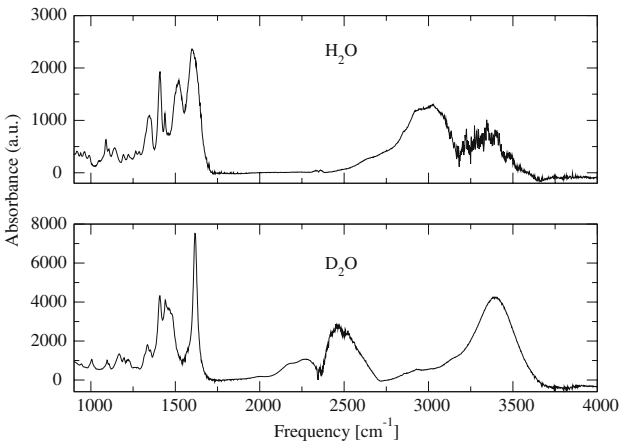

Fig. 9 Experimental infrared spectra of a 0.1 M L-histidine solution in H_2O and D_2O at a pH(D) of 7.6

the position and pattern of the peaks are not in good agreement with the calculated spectra. The calculation was repeated with the larger basis set aug-cc-pVDZ (Fig. 13). These

Table 7 Observed and calculated wavenumbers for the vibrational modes of the L-histidine zwitterion gmm conformer calculated at the 6-31G(d,p) level in the LH13C model in D_2O and H_2O

$\nu_{calculated}$[b]	Assignment[a]$_{PED}$	$\nu_{calculated}$[c]	Assignment[a]$_{PED}$
3,381	q40 0.99	3,206	q38 0.92
3,247	q2 0.99	3,200	q39 0.92
3,206	q38 0.92	3,125	q4 0.52 q5 0.44
3,200	q39 0.92	3,083	q7 0.81 q5 0.14
3,125	q4 0.53 q5 0.44	3,075	q4 0.44 q5 0.40 q7 0.14
3,084	q7 0.83 q5 0.14	2,495	q40 0.96
3,075	q4 0.45 q5 0.41 q7 0.13	2,382	q2 0.95
2,961	q3 0.98	2,186	q3 0.78 q1 0.17
2,896	q1 0.99	2,115	q1 0.80 q3 0.15
1,709	q14 0.81 q16 0.11	1,642	q9 0.53 q8 0.33
1,700	q15 0.81 q17 0.14	1,609	q34 0.49 q6 0.16 q44 0.11
1,646	q9 0.40 q8 0.25 q13 0.19	1,518	q41 0.35 q46 0.25 q37 0.15
1,633	q34 0.38 q48 0.19 q6 0.14	1,494	q21 0.89
1,623	q13 0.63 q9 0.17	1,428	q8 0.32 q11 0.22 q9 0.14 q28 0.13
1,523	q41 0.33 q46 0.26 q37 0.18	1,413	q35 0.35 q37 0.12 q20 0.11
1,498	q21 0.68	1,385	q19 0.51 q24 0.12
1,477	q48 0.28 q21 0.20 q34 0.16 q37 0.11	1,370	q23 0.41 q37 0.11
1,437	q23 0.20 q8 0.20 q11 0.17	1,364	q23 0.29 q41 0.17 q37 0.15
1,402	q23 0.30 q8 0.15 q17 0.10 q9 0.10	1,303	q24 0.34 q20 0.17 q19 0.12
1,398	q41 0.20 q35 0.17 q20 0.15	1,281	q44 0.41 q46 0.15
1,387	q19 0.40	1,269	q24 0.21 q36 0.14 q46 0.12
1,314	q20 0.30	1,236	q13 0.70 q10 0.12
1,303	q24 0.31 q16 0.17 q44 0.11	1,226	q14 0.12 q20 0.11
1,282	q44 0.32 q19 0.12	1,212	q14 0.45 q15 0.32
1,270	q36 0.20 q46 0.11 q35 0.11	1,207	q15 0.43 q14 0.17 q20 0.10
1,240	q17 0.37 q24 0.15 q16 0.15 q23 0.12	1,138	q36 0.53 q44 0.18
1,178	q37 0.36 q48 0.19 q46 0.13	1,090	q12 0.39 q10 0.20
1,151	q20 0.29 q16 0.14 q24 0.11 q23 0.11	1,063	q18 0.16 q27 0.14 q10 0.12
1,137	q36 0.48 q44 0.20	1,026	q17 0.29 q25 0.13 q26 0.11
1,099	q10 0.40 q12 0.23	998	q50 0.31 q35 0.17 q6 0.11
1,027	q50 0.29 q35 0.12 q34 0.11	960	q48 0.32 q51 0.29 q37 0.11 q35 0.10
979	q18 0.21 q12 0.15 q27 0.12	937	q51 0.55 q48 0.30
949	q51 0.80	889	q18 0.25 q17 0.24 q11 0.10
944	q11 0.30 q25 0.11	863	q16 0.38 q12 0.11
874	q53 0.42 q49 0.37 q52 0.12	844	q45 0.23 q18 0.14 q10 0.10 q53 0.10
862	q18 0.26 q10 0.17	828	q45 0.38 q47 0.24 q52 0.20
828	q45 0.35 q52 0.28 q47 0.28	823	q47 0.48 q53 0.14 q45 0.14
821	q47 0.45 q45 0.21	799	q28 0.18 q30 0.14 q50 0.11 q26 0.11
808	q28 0.22 q45 0.13 q30 0.12	715	q30 0.21 q22 0.20 q43 0.20
719	q22 0.20 q30 0.19 q43 0.16		

[a] Assignment of normal modes on PED according to internal coordinates defined in Table 5 followed by the % contribution. Only contributions larger than 0.1 are considered

[b] H_2O

[c] D_2O substitution in all solvent molecules and H12, H18, H19, H_2O in LH

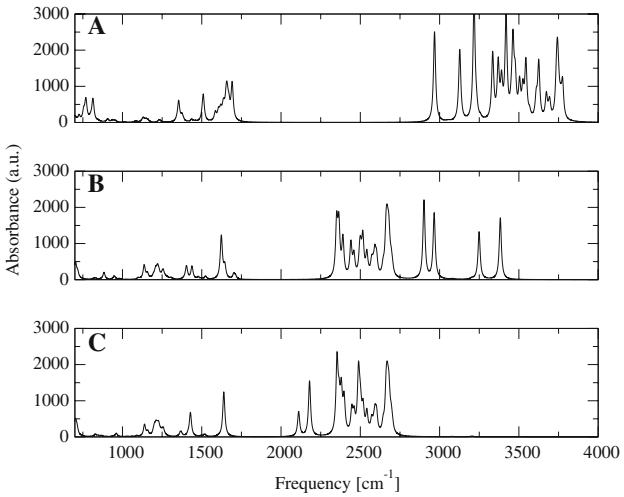

Fig. 10 Vibrational absorption spectra of the L-histidine zwitterion gmm conformer calculated at the 6-31G(d,p) level in the LH13C model with no deuterium substitution (A), deuterium substitution in solvent molecules only (B) and deuterium substitution in both solvent molecules and L-histidine (C)

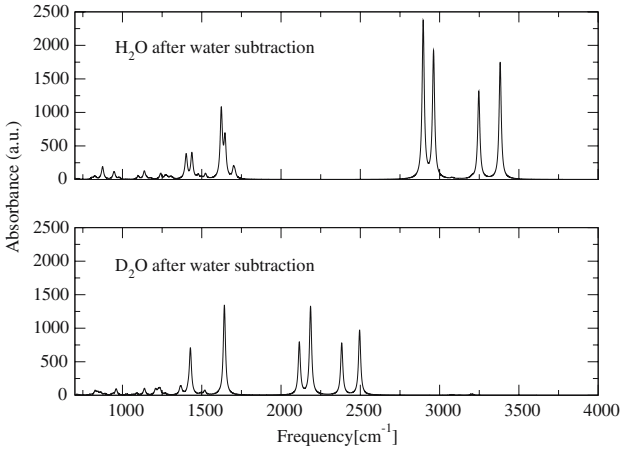

Fig. 11 Vibrational absorption spectra of the L-histidine zwitterion gmm conformer calculated at the 6-31G(d,p) level in the LH13C model in H_2O and D_2O after a theoretical water subtraction

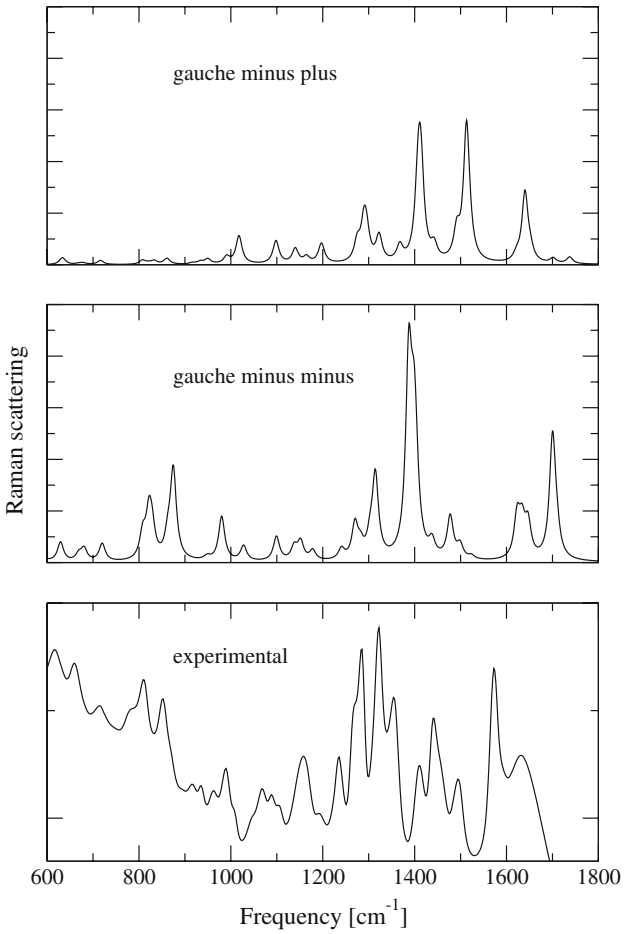

Fig. 12 Raman spectra of the L-histidine zwitterion (gmm and gmp conformers) solvated with 13 explicit water molecules plus PCM continuum model calculated at the B3PW91/6-31G(d) level in comparison to the experimental Raman spectrum of a L-histidine solution

spectra show a much better agreement with the experimental spectrum than the ones in Fig. 12. The peaks in the 1,200–1,600 cm^{-1} region are still shifted to higher frequency compared to the experimental spectrum but the pattern of these peaks shows a better agreement than with the smaller basis set. The presence of a single peak in the 1,300 cm^{-1} region and the pattern of the peaks between 1,200–1,600 cm^{-1} in the gmm conformer suggest that this is the dominant structure in solution, confirming the results from the IR analysis.

3.4.2 Vibrational circular dichroism spectroscopy

The calculated spectra of the gmp and gmm conformers in Fig. 14 indicate that the two structures are distinguishable by their VCD spectra in the 1,000–1,800 cm^{-1} region. The main differences are the patterns in the 1,100–1,300 cm^{-1}, the two peaks around 1,700 cm^{-1} and the orientation of the peak at $\sim$ 1,500 cm^{-1} . Using these three areas a comparison of the theoretical spectra to the experimental one indicates that the spectrum of the gmm conformer is again a better match, confirming the observations from the IR and Raman analysis.

3.4.3 Raman optical activity spectroscopy

The first ROA spectra (Figs. 15,16) were calculated with the LH13C model. Both conformers show poor agreement with the experimental spectrum. This could be due to a number of factors including the smaller basis set used and the position of the explicit waters in the solvation model. The position of the individual solvent molecules has a large effect on the spectra and the experimental spectrum is an average of a large number of different structural combinations. To

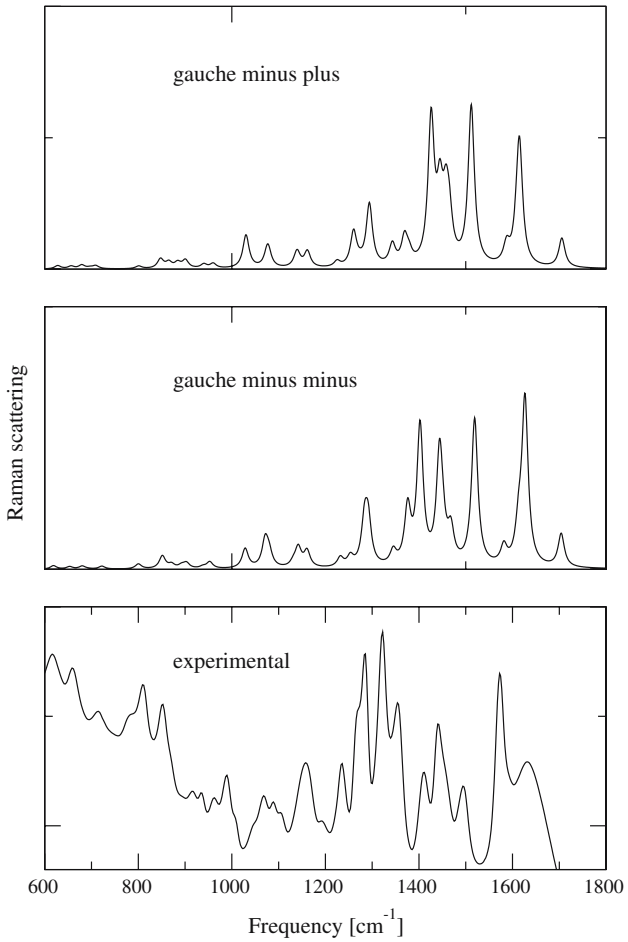

Fig. 13 Raman spectra of the L-histidine zwitterion (gmm and gmp conformers) solvated with 13 explicit water molecules plus PCM continuum model calculated at the B3PW91/aug-cc-pVDZ level after a theoretical water subtraction in comparison to the experimental Raman spectrum of a L-histidine solution

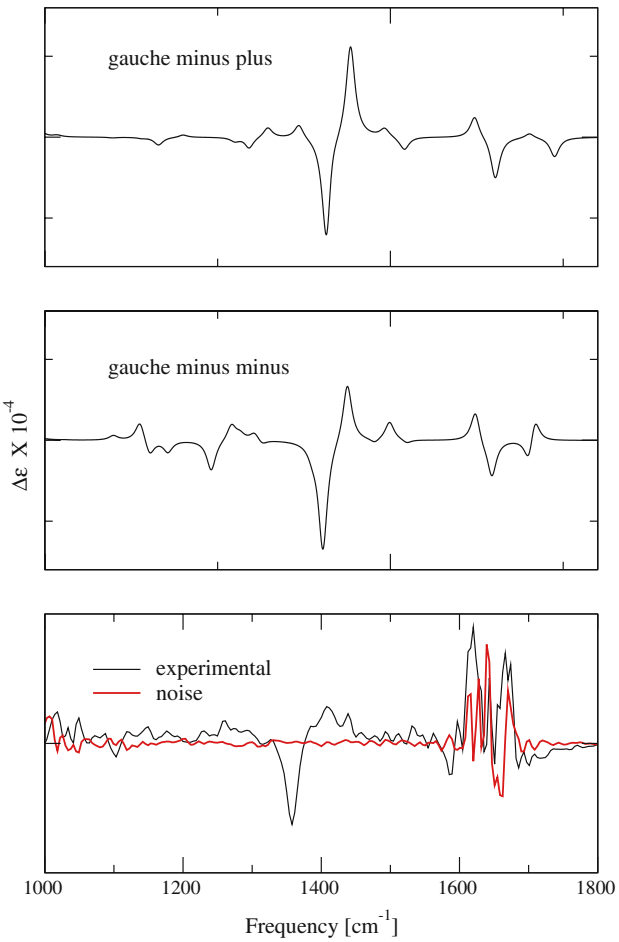

Fig. 14 VCD spectra of the L-histidine zwitterion (gmm and gmp conformers) solvated with 13 explicit water molecules plus PCM continuum model calculated at the B3LYP/6-31G(d) level after a theoretical water subtraction in comparison to the experimental spectrum of a L-histidine solution

average out the position of the water molecules the spectra for a large number of different positions of the solvent cluster, evaluated using molecular dynamics simulations, could be considered. As this is a resource expensive task the explicit solvent molecules were removed. The calculations were repeated by using a LH structure that was optimised in the presence of the explicit water molecules but the LH was only solvated with the PCM continuum model during the calculation of the Raman frequency and Intensities (Figs. 17, 18). These spectra show much better agreement with the experimental spectrum suggesting that the position of the water molecules had a large effect in the first set of calculations. Encouraged by these results the calculations were carried out using the larger basis set aug-cc-pVDZ (Figs. 19, 20). These spectra show an even better match to the experimental measurements. A comparison of CID3 in Fig. 19 and Fig. 20 shows that the ROA spectra of the two conformers are very similar. For the pattern in the 1,300–1,500 cm^{-1} region the gmp shows a slightly better agreement while the gmm spectra is a better match in the 500–900 cm^{-1} region, suggesting that both conformers are present in solution. A comparison of the relative energies of the two conformers at this level of theory shows that the gmm is only slightly (6 kJ/mol) lower in energy than the gmp conformer supporting the argument that both species coexist in solution.

4 Summary and conclusion

In this study six different conformers of the LH zwitterion have been solvated with five different solvation models to simulate the effect of both bulk water and the hydrogen bonded cluster formed by explicit water molecules. The bulk water was modeled using the dielectric continuum model COSMO and PCM while the cluster was simulated by the addition of 13 or 17 water molecules. The geometries of the

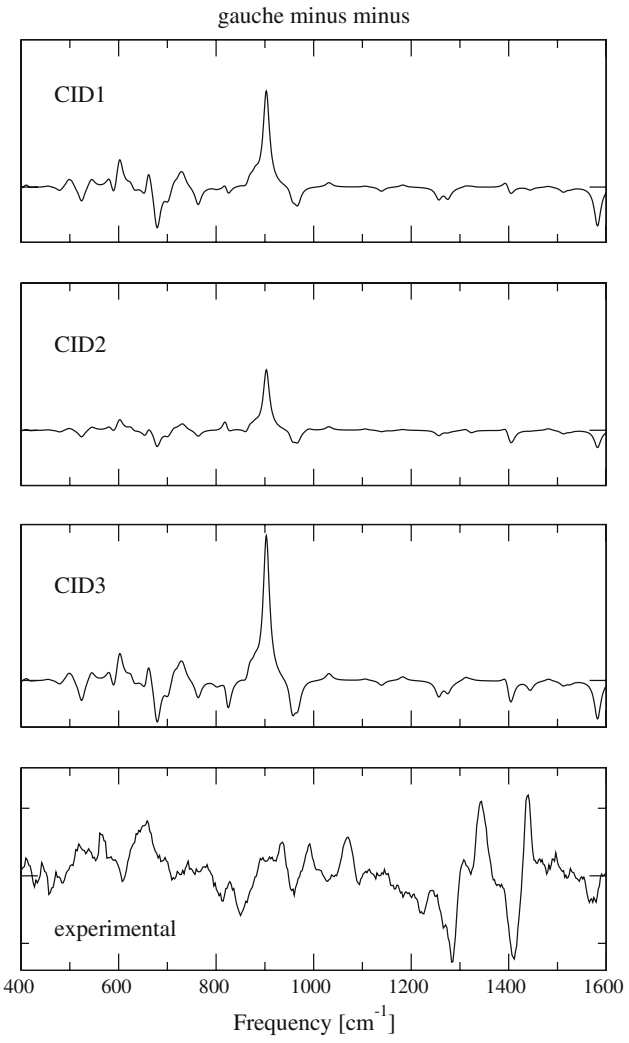

Fig. 15 ROA of the L-histidine zwitterion (gmm conformer) solvated with 13 explicit water molecules plus PCM continuum model calculated at the B3LYP/6-31G(d) level in comparison to the experimental spectrum of a L-histidine solution

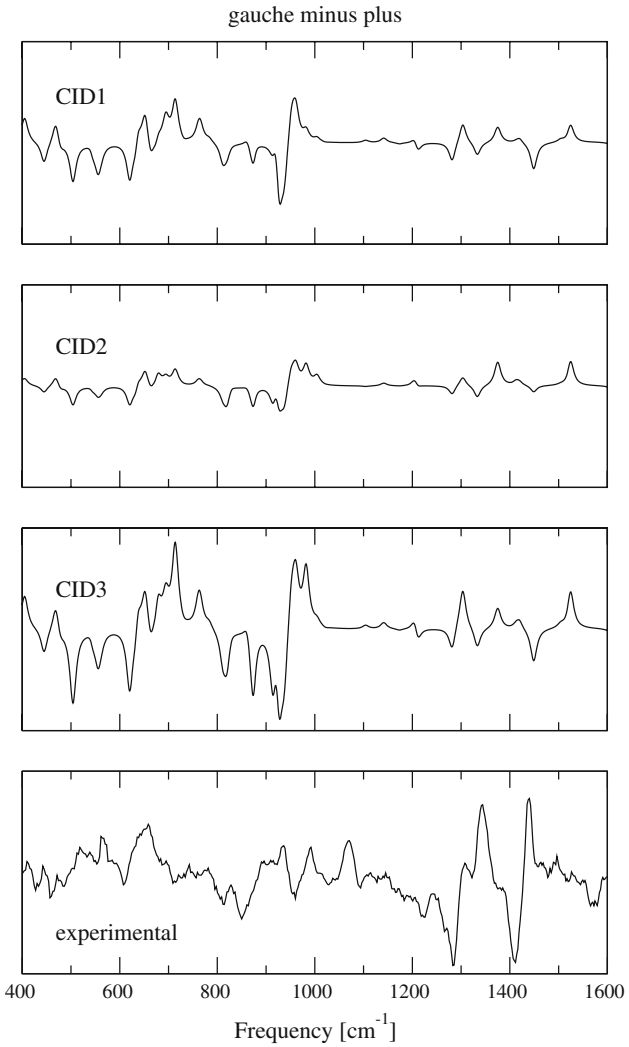

Fig. 16 ROA spectra of the L-histidine zwitterion (gmp conformer) solvated with 13 explicit water molecules plus PCM continuum model calculated at the B3LYP/6-31G(d) level in comparison to the experimental spectrum of a L-histidine solution

initial structures have been optimised at the OPBE0/DZP level using the three solvation models. The results show that the zwitterion is not stable in the gas phase and confirm the stabilizing effect of solvation previously reported for other amino acids. The effect of the different solvation models on the geometrical parameters has been shown by numerical comparison of the bond lengths, dihedral angels and relative energies of the six conformers. The results confirm previously reported observations that the structural parameters are substantially affected by solvating the molecule and that the relative energies of the conformers should not be used as a sole parameter to determine which structure is present in solution.

The VA spectrum of the trans minus conformer has been calculated in all five solvation models to demonstrate the solvation effect on the spectra of the LH zwitterion. The continuum model and the explicit water molecules show different effects on the spectra reflecting that the models simulate different solvent effects. The areas most affected by the addition of the solvation models are the bands of the polar functional groups COO^- and NH_3^+. The addition of explicit water molecules adds a large number of new bands to the spectra demonstrating the effect of the coupling between the solvent and the LH while the continuum model results in increased intensities giving the impression of broader bands. The results showed that the use of the combination model employing both explicit water molecules and a continuum model produces a spectrum with the best agreement to the experimental spectra. The addition of more water molecules does not affect the spectra substantially but increases the cost of computation. These results again demonstrate that solvation has a substantial effect on the spectral properties

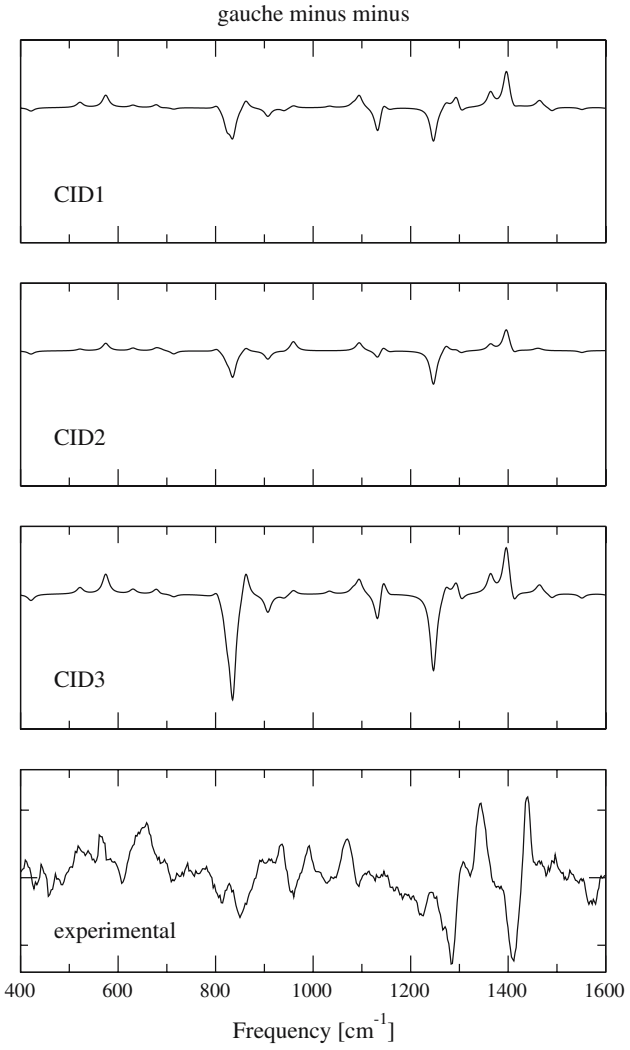

Fig. 17 ROA spectra of the L-histidine zwitterion (gmm conformer) solvated with the PCM continuum model calculated at the B3PW91/6-31G(d) level in comparison to the experimental spectrum of a L-histidine solution

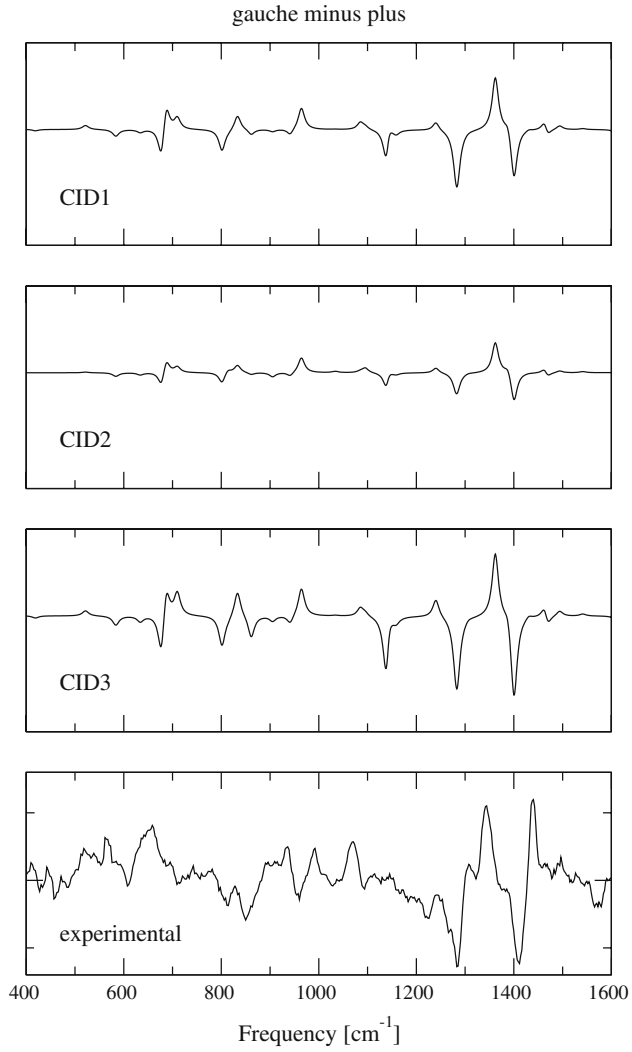

Fig. 18 ROA spectra of the L-histidine zwitterion (gmp conformer) solvated with the PCM continuum model calculated at the B3PW91/6-31G(d) level in comparison to the experimental spectrum of a L-histidine solution

and calculations like these should not be modeled in the gas phase. Future calculations would benefit from the use of molecular dynamic simulations for the determination of the position and number of water molecules in the first hydration shell. The results also showed that a change in the basis set affects the position and intensities of bands. A larger basis set produced a better agreement with the experimental spectrum, especially for the modes of the polar groups that build the characteristic bands of the spectrum.

A comparison of the VA spectra of the six conformers of the LH zwitterion suggests that the different structures exhibit some characteristic features that enables their differentiation. This allows some preliminary conclusions regarding which structure is present in solution. The gmm conformer showed the best agreement to the experimental spectrum, confirming the results from the relative energies of the optimised structures in the LH13C model. The possibility of more than one conformer being present in solution should also be considered.

A theoretical water subtraction has been performed on the two lowest energy structures (gmm and gmp) calculated in the LH13C model at the 6-31G(d,p) level. A set of internal coordinates has been defined for the LH zwitterion and the normal modes have been assigned using a PED. Water subtraction simplifies the spectra and, in combination with the PED, facilitates the assignment of bands. The isolation of the histidine bands also enables a more detailed comparison of the conformers and the identification of characteristic bands but still allows the solvent effect to be considered in the calculation. The VA spectrum of the gmm conformer in D_2O has been calculated. The results showed that deuterium substitution mostly affected the bands from the NH_3^+ group. The

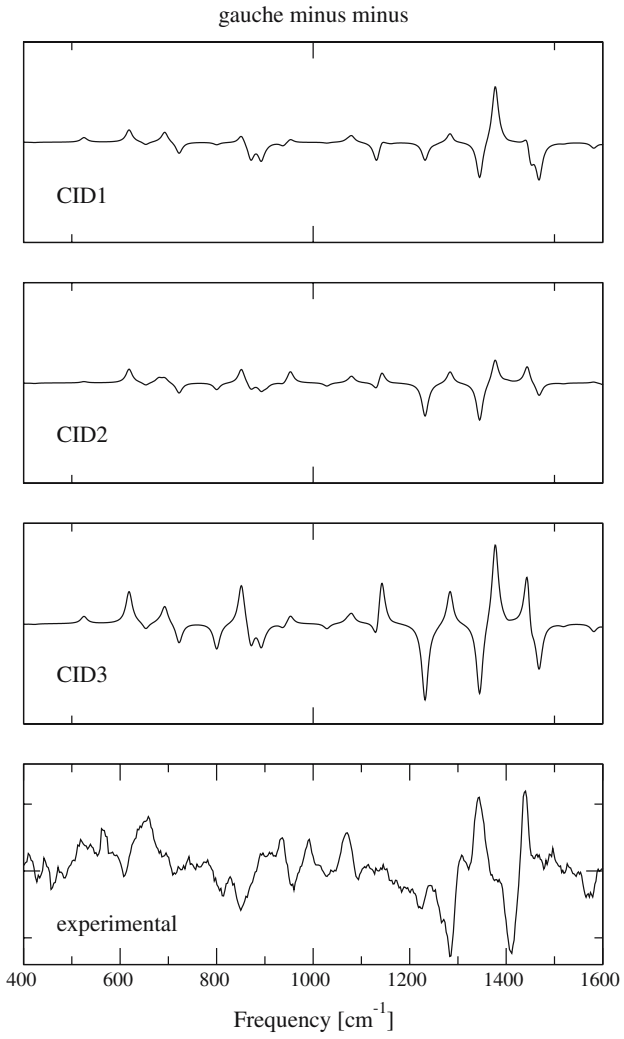

Fig. 19 ROA spectra of the L-histidine zwitterion (gmm conformer) solvated with the PCM continuum model calculated at the B3PW91/aug-cc-pVDZ level in comparison to the experimental spectrum of a L-histidine solution

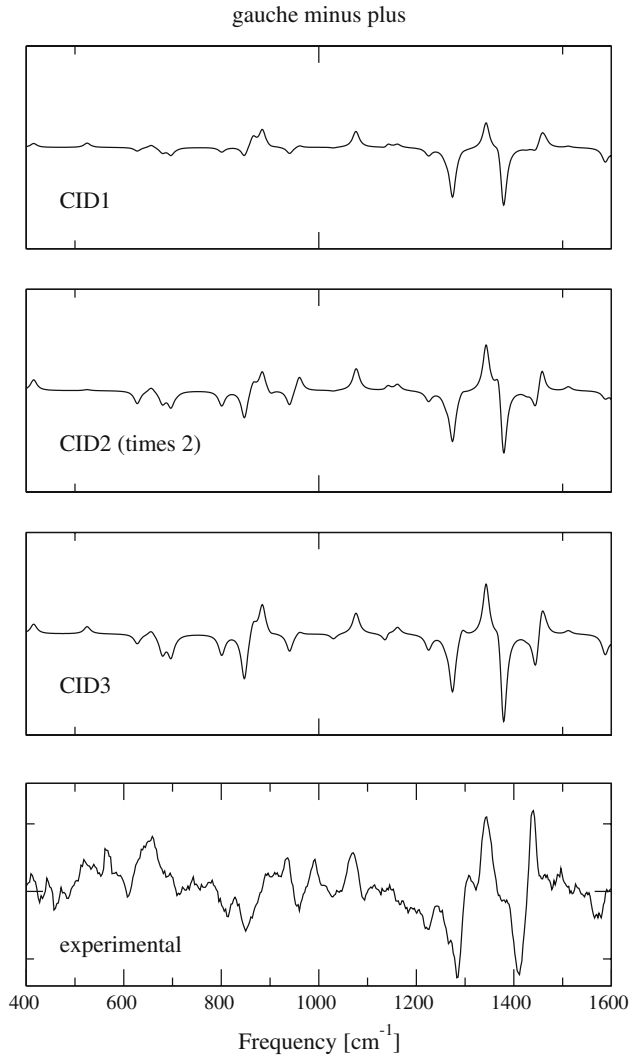

Fig. 20 Raman optical activity spectra of the L-histidine zwitterion (gmp conformer) solvated with the PCM continuum model calculated at the B3PW91/aug-cc-pVDZ level in comparison to the experimental spectrum of a L-histidine solution

shift of the bands from their position in water can be used to isolate the bands of the histidine molecule and when used with a PED can assist in the identification and confirmation of band assignment.

A comparison of the calculated Raman and VCD spectra with their experimental measurements confirmed the results of the IR analysis, that the gmm conformer is the dominant species in solution. The results from the ROA experiments suggest that both conformers are present in solution.

This study shows the efficacy of adding explicit water molecules to the simulation of the VA spectra of amino acids in aqueous solution. The use of VA/IR spectroscopy could prove to be a viable method for the structural characterization of amino acids in solution, especially when combined with VCD, Raman scattering and ROA, electronic absorption (EA), electronic circular dichroism (ECD) and theoretical modeling studies (classical MD, BOMD, DFT and TDDFT simulation of the structures which are predicted to be present). The inverse problem, of determining the structures only from the spectra is an ongoing problem in our as well as other laboratories around the world. Prof. T. A. Keiderling's group in Chicago, Illinois, has used an alternative approach (see the contribution of the Keiderling group in this special issue of TCA and references therein).

Acknowledgments The authors would like to thank the ARC (Australian Research Council) LEIF program for the funding to purchase the FTIR instrument which was used to measure the IR spectra. Additionally the authors would like to thank the Western Australia supercomputer center, iVEC, and the Australian Partnership for Advanced Computing (APAC) National Facility, the Finnish Supercomputer Center (CSC) in Espoo, Finland and the Laboratory of Physics at Helsinki University of Technology for computer time and resources.

We would also like to thank R. M. Nieminen, I. M. Degtyarenko and J. D. Gale for interesting and thought provoking discussions concerning the modeling of biomolecules like LH in their native and non-native environments. Finally, K. J. Jalkanen would like to thank the Western Australian government for funding for the Premier's Research Fellow program which supported his stay at the NRI in Perth, WA.

References

1. Mesu JG, Visser T, Soulimani F, Weckhuysen BM (2005) Vib Spectrosc 39:114
2. Hasegawa K, Ono T, Noguchi T (2000) J Phys Chem B 104:4253
3. Wellner N, Zundel G (1994) J Mol Struct 317:249
4. Hashimoto S, Takeuchi H (1998) J Am Chem Soc 120:11012
5. Hashimoto S, Ono K, Takeuchi H (1998) J Raman Spectrosc 29:969
6. Wang D, Zhao X, Vargek M, Spiro T (2000) J Am Chem Soc 122:2193
7. Frey PA, Whitt SA, Tobin J (1994) Science 264:1927
8. Marti EM, Methivier C, Dubot P, Pradier CM (2003) J Phys Chem B 107:10785
9. Miura T, Satoh T, Hori-I A, Takeuchi H (1998) Biol Chem 38:11560
10. Miura T, Satoh T, Hori-I A, Takeuchi H (1998) J Raman Spectrosc 29:41
11. Vargek M, Zhao X, Lai Z, McLendon G, Spiro T (1998) Inorg Chem 38:1372
12. Hudáky P, Perczel A (2004) J Phys Chem A 108:6195
13. Wolpert M, Hellwig P (2006) Spectrochim Acta A 64:987
14. Takeuchi H (2003) Biopolymers (Biospectrosc) 72:305
15. Tasumi M, Harada I, Takamatsu T, Takahashi S (1982) J Raman Spectrosc 12:149
16. Toyama A, Ono K, Hashimoto S, Takeuchi H (2002) J Phys Chem B 106:3403
17. Majoube M, Millié Ph, Vergoten G (1995) J Mol Struct 344:21
18. Gallouj H, Lagant P, Vergoten G (1997) J Raman Spectrosc 28:909
19. Poon C, Samulski E, Weise CF, Weisshaar JC (2000) J Am Chem Soc 122:5642
20. Hashimoto S, Takeuchi H (2006) Biochemistry 45:9660
21. Zhao X, Wang D, Spiro T (1998) J Am Chem Soc 120:8517
22. Jalkanen KJ, Jürgensen VW, Claussen A, Rahim A, Jensen GM, Wade RC, Nardi F, Jung C, Degtyarenko IM, Nieminen RM, Herrmann F, Knapp-Mohammady M, Niehaus TA, Frimand K, Suhai S (2006) Int J Quantum Chem 106:1160
23. Jürgensen VW, Jalkanen KJ (2006) Phys Biol 3:S63
24. Abdali S, Jalkanen KJ, Bohr H, Suhai S, Nieminen RM (2002) Chem Phys 282:219
25. Han WG, Jalkanen KJ, Elstner M, Suhai S (1998) J Phys Chem B 102: 2587
26. Frimand K, Bohr H, Jalkanen KJ, Suhai S (2000) Chem Phys 255:165
27. Tajkhorshid E, Jalkanen KJ, Suhai S (1998) J Phys Chem 102:5899
28. Jalkanen KJ, Nieminen RM, Frimand K, Bohr J, Bohr H, Wade RC, Tajkhorshid E, Suhai S (2001) Chem Phys 265:125
29. Jalkanen KJ, Nieminen RM, Knapp-Mohammady M, Suhai S (2003) Int J Quantum Chem 92:239
30. Madison V, Kopple KD (1980) J Am Chem Soc 102:4855
31. Knapp-Mohammady M, Jalkanen KJ, Nardi F, Wade RC, Suhai S (1999) Chem Phys 240:63
32. Weinhold F, (1997) J Mol Struct Theochem 398–399:181
33. Smith P (1999) J Chem Phys 111:5568
34. Jalkanen KJ, Suhai S (1996) J Phys Chem 208:81
35. Deng Z, Polavarapu PL, Ford SJ, Hecht L, Barron LD, Ewig CS, Jalkanen KJ (1996) J Phys Chem 100:2025
36. Jalkanen KJ, Elstner M, Suhai S (2004) J Mol Struct (Theochem) 675:61
37. Perkins SJ (2001) Biophy Chem 93:129
38. Gerstein M, Chothia C (1996) Proc Natl Acad Sci USA 93:10167
39. Marechal Y (1996) Faraday Discuss 103:349
40. te Velde G, Bickelhaupt FM, Baerends EJ, Guerra FC, van Gisbergen SJA, Snijders JG, Ziegler T (2001) J Comp Chem 22:931 (see also Nicu VP, Neugebauer J, Wolff SF, Baerends EJ (2007) Theor Chem Acc doi:10.1007/s00214-006-0234-x (this issue)
41. Nafie LA (2006) Infrared and Raman vibrational optical activity: pharmaceutical and biological applications presented at the American Chemical Society 232nd national meeting, San Francisco, CA USA, 14 September, 2006. In: Division of Biochemical Technology, talk no.: 451:42.
42. Eker F, Cao X, Nafie LA, Huang Q, Schweitzer-Stenner (2003) J Phys Chem B 107:358
43. Huang Z, Yu W, Lin Z (2006) J Mol Struct (THEOCHEM) 801:7
44. Schaftenaar G (2006) http://www.cmbi.ru.nl/molden/molden.html
45. Degtyarenko IM, Jalkanen KJ, Gurtovenko AA, Nieminen RM (2007) J Phys Chem B doi:10.1021/jp0676991
46. Jalkanen KJ, Nieminen RM, Bohr J (2000) Vestnik Moskovskogo Universiteta. Khimiya 41:4
47. Pulay P, Gogarasi G, Pang F, Boggs JE (1979) J Am Chem Soc 101:2550